Resummation of combined QCD-electroweak effects in Drell Yan lepton-pair production

Luca Buonocore [ID],[a] **Luca Rottoli** [ID][b] **and Paolo Torrielli** [ID][c]

[a]*CERN, Theoretical Physics Department,*
CH-1211 Geneva 23, Switzerland

[b]*Department of Physics, University of Zürich,*
CH-8057 Zürich, Switzerland

[c]*Dipartimento di Fisica, Università di Torino, and INFN, Sezione di Torino,*
Via P. Giuria 1, I-10125 Torino, Italy

E-mail: lbuonocor@cern.ch, luca.rottoli@physik.uzh.ch,
torriell@to.infn.it

ABSTRACT: We consider neutral- and charged-current Drell Yan lepton-pair production at hadron colliders, and include dominant classes of electroweak and mixed QCD-electroweak corrections to all orders in perturbation theory. The accurate description of these physical effects is vital for a precise determination of fundamental Standard Model parameters, such as the W-boson mass and the electroweak mixing angle, as well as for a solid assessment of the associated theoretical uncertainties. Our state-of-the-art resummation reaches next-to-leading-logarithmic accuracy in both the electroweak and the mixed QCD-electroweak perturbative expansions, including constant terms at first order beyond Born level in both couplings, i.e. at order α and $\alpha_s \alpha$. These effects are incorporated on top of QCD predictions at next-to-next-to-next-to-leading-logarithmic accuracy, which include constant terms at third order in the strong coupling. Our results retain, for the first time at this accuracy, full dependence on the kinematics of the final-state leptons, thereby enabling a realistic comparison with experimental analyses at the differential level in presence of fiducial cuts. We present a phenomenological analysis of the impact of electroweak corrections in relevant observables at the LHC. We find visible shape distortions in resummation-dominated kinematical regions with respect to pure-QCD predictions, highlighting the importance of a complete description, not limited to QCD, for precision Drell Yan physics.

Contents

1   Introduction

The production of lepton pairs through the Drell Yan (DY) mechanism is central to the precision physics programme of hadron colliders such as the Tevatron and the LHC. Owing to its large cross section and its clean experimental signature, with at least one hard charged lepton in the final state, the DY process features prominently in the precise determination of fundamental Standard Model (SM) parameters, such as the W-boson mass [1–5], the electroweak (EW) mixing angle [6–12], and the strong coupling [13]. Moreover, it provides stringent constraints on parton distribution functions (PDFs) of the proton, and represents a dominant background for many signals, both within and beyond the SM.

On the theoretical side, it is crucial to provide predictions of the highest accuracy for DY fiducial cross sections and differential distributions. Given the level of accuracy attained nowadays by experimental measurements [14–20], not only does this imply the account of QCD radiative corrections at high perturbative orders, but also the inclusion of EW contributions, whether they are pure EW effects or QCD-EW interferences.

At fixed order in QCD perturbation theory, after pioneering next-to-leading-order (NLO) and next-to-NLO (NNLO) inclusive DY calculations [21–23], differential results became available at NNLO [24–29]. Nowadays, the next-to-NNLO (N^3LO) level has been reached both for total rates [30–32], and for differential distributions [33–39]. The NLO EW corrections have been calculated long ago for charged-current DY (CCDY) in refs. [40–44] and for neutral-current DY (NCDY) in refs. [45–49]. Efforts to go beyond that level have witnessed a revived interest in recent years, with the calculation of NNLO mixed QCD-EW effects. First results have been obtained in the *pole* approximation (see ref. [50] for a general discussion) with the calculation in refs. [51, 52] of the so-called *factorisable* contributions of *initial-final* and *final-final* type. More recently, the missing *initial-initial* contributions have been considered in ref. [53]. Going beyond the pole approximation, mixed QCD-QED corrections were obtained

in refs. [54, 55] for the inclusive production of an on-shell Z boson, and in ref. [56] for off-shell Z boson production and decay into a pair of neutrinos at the fully differential level. Mixed QCD-EW $\mathcal{O}(\alpha_s\alpha)$ double-real corrections were obtained in [57] for on-shell Z and W production, while the complete $\mathcal{O}(\alpha_s\alpha)$ computation for the production of on-shell Z bosons has been presented in refs. [58, 59]. For the off-shell case, there is a computation [60] of the mixed QCD-EW corrections to CCDY, where all contributions are evaluated exactly except for the finite part of the two-loop amplitude, which was evaluated in the pole approximation. As for NCDY, thanks to the calculation of its exact two-loop amplitude [61, 62], the complete mixed QCD-EW corrections have been achieved in refs. [63, 64].

It is well known that predictions at fixed order in perturbation theory are reliable only for sufficiently inclusive quantities. Whenever an observable is sensitive to infrared and/or collinear (IRC) radiation, large logarithms arise in the calculation of its higher-order corrections, featuring as argument the ratio of a hard to an IRC scale. The presence of such logarithms spoils the convergence of the perturbative expansion, and claims for a resummation of logarithmic enhancements to all perturbative orders. In the case of QCD corrections to the DY process, the resummation of IRC-sensitive observables like the lepton-pair transverse momentum $p_t^{\ell\ell}$ or the ϕ_η^* distribution [65] has seen a steady evolution, from seminal papers [66–70] to more recent developments in a variety of formalisms [71–83], reaching nowadays the standard of next-to-next-to-next-to-leading-logarithmic (N³LL) accuracy [39, 84–93], with some next-to-N³LL (i.e. N⁴LL) elements approximately encoded in some cases [37, 38, 94, 95]. The inclusion of QED multiple emissions and virtual EW effects in the paradigm of analytic resummation has been considered more recently. Early work [96] and phenomenological studies [97, 98] were produced focusing on the impact of EW corrections on precision CCDY observables. Analytic ingredients for a mixed-coupling resummation were computed in [99–101]. A combination of QCD, QED and mixed QCD-QED resummations was achieved in [102, 103] for on-shell Z and W production, respectively, i.e. without taking into account leptonic decay products. QED resummation effects at the level of final-state leptons have been so far available only through dedicated QED shower programs such as PHOTOS [104] and HORACE [105, 106], including the possibility to match with fixed order NLO-EW results, or general-purpose Monte Carlo event generators as PYTHIA8/VINCIA [107–109], HERWIG7 [110, 111] and SHERPA [112–114]. These tools, however, typically feature a quite low logarithmic accuracy, which may be a limiting factor for their use in high-precision phenomenology. In this context, the state of art is represented by matched calculations which include a combination of factorisable effects of both QCD and EW origin, and preserve the NLO-QCD and NLO-EW accuracy for inclusive quantities with respect to additional radiation [115–119].

In this article we take a step forward in the inclusion of EW effects in the DY process. We present a highly accurate combination of QCD, EW, and mixed QCD-EW resummations for DY production at the level of final-state lepton pairs, derived in the RADISH framework [78, 84, 91]. Our predictions include all necessary terms for a next-to-leading-logarithmic (NLL) resummation in the EW coupling constant α, as well as in the mixed QCD-EW expansion $\alpha_s\alpha$, on top of retaining N³LL QCD accuracy. First-order constant terms in the EW and in the mixed expansions, as well as third-order constant terms in QCD, are also included,

paving the way to a state-of-the-art matching of resummed predictions with fixed-order calculations. The capability of describing final-state leptons is unavoidable to realistically match the setup of experimental DY analyses, which feature fiducial acceptance cuts on the leptonic system. Our results allow one to assess at unprecedented accuracy the impact of all-order mixed QCD-EW corrections on leptonic observables, such as the charged-lepton transverse momentum, the lepton-pair transverse mass, or the jacobian asymmetry [120, 121], relevant for W-mass determination. Moreover, they open the door to the exploration of EW effects in different resummation environments, still available in RADISH, such as jet-vetos or double-differential resummations [122, 123], or for other scattering processes.

The article is organised as follows. In section 2 we concisely review the RADISH resummmation formalism, and detail how EW and mixed QCD-EW effects are consistently included at NLL accuracy. In section 3 we describe the validation of our results. Section 4 collects our phenomenological predictions at the LHC, both for neutral- and for charged-current DY. Finally, we draw our conclusions in section 5. Appendix A collects formulæ relevant for the employed theoretical framework.

2 Inclusion of EW and mixed QCD-EW effects in RADISH

The RADISH formalism [78, 84, 91] is designed for the all-order resummation of enhanced logarithmic effects in global recursively infrared- and collinear- (rIRC) safe [124–126] observables that vanish away from the Sudakov limit. Notable observables in this class include for instance the transverse momentum of the final-state Drell Yan leptonic system, where the limit of small observable is determined [66] by azimuthal cancellations among the emitted radiation. The formalism is based on a physical picture in which hard particles incoming to or outgoing from a primary scattering coherently radiate an ensemble of soft and collinear partons. The resummation is performed in momentum space, as opposed to conventional impact-parameter (b) space, namely the expressions are directly written in terms of the momenta of the radiated partons.

Radiative effects on rIRC-safe observables can be systematically classified according to the perturbative logarithmic order at which they enter. We denote with V the considered observable, that we assume to be dimensionless without loss of generality. $\Sigma(v)$ represents the cumulative cross section for V being smaller than v. In a gauge theory with coupling a, the counting of logarithms is performed at the level of $\ln \Sigma(v)$, where terms of order $a^n \ln(1/v)^{n+1-k}$ are ranked as (next-to)^k-leading logarithmic (N^{k}LL), n and k being positive integers.

Focusing first on the case of QCD, with $a = \alpha_s(\mu_R) \equiv \alpha_s$, the strong coupling at the renormalisation scale μ_R, the RADISH formula for the resummation of V in colour-singlet production can be schematically written as

$$\frac{\mathrm{d}\Sigma(v)}{\mathrm{d}\Phi_B} = \int \frac{\mathrm{d}k_{t1}}{k_{t1}} \mathcal{L}(k_{t1}) \, \mathrm{e}^{-R(k_{t1})} \, \mathcal{F}(v, \Phi_B, k_{t1}) \,, \tag{2.1}$$

where the expression is fully differential with respect to the Born phase-space variables Φ_B, which allows for the application of fiducial cuts to match experimental acceptance.

The Sudakov radiator $R(k_{t1})$ is defined as

$$R(k_{t1}) = \sum_{\ell=1}^{2} R_\ell(k_{t1}), \qquad R_\ell(k_{t1}) = \int_{k_{t1}}^{M} \frac{\mathrm{d}q}{q} \left[A_\ell(\alpha_s(q)) \ln \frac{M^2}{q^2} + B_\ell(\alpha_s(q)) \right], \qquad (2.2)$$

where k_{t1} denotes the transverse momentum of the hardest radiation in the ensemble of emitted QCD partons, while M is the hard scale of the process, e.g. the lepton-pair invariant mass for Drell Yan. A_ℓ, B_ℓ are flavour-conserving soft-collinear and hard-collinear anomalous dimensions with a well-defined perturbative expansion:

$$A_\ell(\alpha_s) = \sum_{n=1}^{\infty} \left(\frac{\alpha_s}{2\pi}\right)^n A_\ell^{(n)}, \qquad B_\ell(\alpha_s) = \sum_{n=1}^{\infty} \left(\frac{\alpha_s}{2\pi}\right)^n B_\ell^{(n)}. \qquad (2.3)$$

In the above formulæ, ℓ labels the hard legs responsible for radiation, with $\ell = 1, 2$ for the initial-state radiation relevant to colour-singlet production in QCD. The dependence upon the flavour of the hard legs is encoded in the values of the corresponding anomalous dimensions A_ℓ and B_ℓ. The evaluation of the integral in eq. (2.2) yields

$$R(k_{t1}) = -L\, g_1(\lambda) - \sum_{n=0}^{\infty} \left(\frac{\alpha_s}{\pi}\right)^n g_{n+2}(\lambda), \qquad (2.4)$$

where $\lambda = \alpha_s \beta_0 L$, and β_0 is the first coefficient of the QCD beta function. Here $L = \ln(Q/k_{t1})$, with Q being the resummation scale, namely a hard scale of the order of M, whose variations allow one to estimate the impact of missing higher-order logarithmic towers. Explicit expressions for the $g_{1,2}(\lambda)$ functions, as well as for the corresponding anomalous dimensions are collected in appendix A, while functions $g_{3,4}(\lambda)$ were presented in appendix B of [84].

The luminosity factor $\mathcal{L}(k_{t1})$ in eq. (2.1) incorporates the Born matrix element and PDF combination, as well as the hard virtual function $H(\mu_R)$ and collinear coefficient functions $C_{ab}(z)$:

$$\mathcal{L}(k_{t1}) = \sum_{c,d} |\mathcal{M}_B|_{cd}^2 \sum_i \left[C_{ci} \otimes f_i(k_{t1}) \right](x_1) \sum_j \left[C_{dj} \otimes f_j(k_{t1}) \right](x_2)\, H(\mu_R), \qquad (2.5)$$

where the convolution is defined by $[f \otimes g](x) = \int_x^1 \frac{\mathrm{d}z}{z} f(z)\, g(x/z)$, and

$$C_{ab}(z) = \delta_{ab}\, \delta(1-z) + \sum_{n=1}^{\infty} \left(\frac{\alpha_s}{2\pi}\right)^n C_{ab}^{(n)}(z),$$

$$H(\mu_R) = 1 + \sum_{n=1}^{\infty} \left(\frac{\alpha_s}{2\pi}\right)^n H^{(n)}(\mu_R). \qquad (2.6)$$

In eq. (2.5) the sums run over all flavour combinations relevant to the considered process, $|\mathcal{M}_B|_{cd}^2$ is the Born squared matrix element, and $f_i(k_{t1})$ are the parton densities evaluated at scale k_{t1}. As customary in the RADISH approach, see e.g. [84], the hard factor $H(\mu_R)$ in eq. (2.6) also includes constant contributions stemming from the Sudakov radiator, expanded out at the appropriate order in the coupling constants: these originate from the introduction of a resummation scale $Q \neq M$ in the definition of the resummed logarithm L, whence they

induce an explicit dependence on Q and M in $H(\mu_R)$. Moreover, all factors of $\alpha_s(k_{t1})$ and $f_k(k_{t1})$ appearing in the luminosity $\mathcal{L}(k_{t1})$ are rewritten in terms of $\alpha_s(\mu_R e^{-L})$ and $f_k(\mu_F e^{-L})$, with μ_F being the factorisation scale, and then perturbatively expanded. As a consequence, the $C_{ab}(z)$ coefficient functions in eq. (2.6) acquire an explicit dependence on Q, μ_F, and μ_R. The evolution of PDFs between different scales is ruled by the DGLAP [127–129] equation

$$\frac{\partial f_i(\mu, x)}{\partial \ln \mu} = \frac{\alpha_s(\mu)}{\pi} \Big[\hat{P}_{ij} \otimes f_j(\mu)\Big](x), \qquad \hat{P}_{ij}(z) = \sum_{n=0}^{\infty} \Big(\frac{\alpha_s}{2\pi}\Big)^n \hat{P}_{ij}^{(n)}(z), \qquad (2.7)$$

in terms of the regularised splitting functions $\hat{P}_{ij}$.

The last ingredient in eq. (2.1) is the radiative function $\mathcal{F}(v, \Phi_B, k_{t1})$, describing an arbitrary number of resolved soft and/or collinear real emissions with a transverse momentum smaller than k_{t1}, starting at NLL accuracy. An explicit expression for this function is not relevant for the present discussion, and will not be derived here. It can however be extracted from the detailed construction of [84, 91]. The interested reader can refer to formula (3.33) of ref. [91] for the evaluation of eq. (2.1) up to N^3LL' order in QCD, using the ingredients calculated in [130–147]. N^3LL' accuracy gives control over all logarithmic towers up to $\alpha_s^n \ln(1/v)^{n-2}$, as well as all terms of order $\alpha_s^n \ln(1/v)^{2n-6}$ in the expanded cumulative cross section. We consider that equation as our baseline QCD resummation formula, and focus on the elements necessary to augment it with EW effects.

Logarithmically enhanced QED and mixed QCD-EW contributions stem from different sources. We aim at reaching NLL accuracy in the mixed coupling expansion, namely at correctly resumming all terms of order $\alpha_s^n \alpha^m \ln(1/v)^{n+m}$, with $\alpha = \alpha(\mu_R)$ the QED running coupling evaluated at the renormalisation scale.

The first effect we consider is the QED contribution to the Sudakov radiator relevant to hard leg ℓ. Analogously to eq. (2.2), we have

$$R_\ell^{\text{QED}}(k_{t1}) = \int_{k_{t1}}^{M} \frac{\mathrm{d}q}{q} \left[A_\ell'(\alpha(q)) \ln \frac{M^2}{q^2} + B_\ell'(\alpha(q)) \right], \qquad (2.8)$$

where A_ℓ' and B_ℓ' are the abelian versions [99, 100] of the corresponding QCD anomalous dimensions:

$$A_\ell'(\alpha) = \sum_{n=1}^{\infty} \Big(\frac{\alpha}{2\pi}\Big)^n A_\ell'^{(n)}, \qquad B_\ell'(\alpha) = \sum_{n=1}^{\infty} \Big(\frac{\alpha}{2\pi}\Big)^n B_\ell'^{(n)}. \qquad (2.9)$$

Since the Drell Yan process features more than two charged particles at Born level, soft wide-angle QED radiation introduces correlations among the hard legs, namely it cannot be described as the incoherent sum of single-leg contributions. This effect, starting at NLL QED accuracy (i.e. $\alpha^n \ln(1/v)^n$), is accounted for by including a radiative function $D'(\alpha(q), \Phi_B)$ in the Sudakov exponent [103, 148], with a QED perturbative expansion:

$$D'(\alpha, \Phi_B) = \sum_{n=1}^{\infty} \Big(\frac{\alpha}{2\pi}\Big)^n D'^{(n)}(\Phi_B). \qquad (2.10)$$

As the notation suggests, such a function carries an explicit dependence upon the Born kinematics, through the invariant masses of charge-correlated pairs. Its expression for *massive* charged leptons, such as the ones we consider throughout this article, can be deduced as the

abelian version of the corresponding QCD function relevant for heavy-quark production [148]. We stress that a finite charged-lepton mass is necessary in order to apply our resummation formalism as is. Explicit logarithms of the mass are generated in the $D'(\alpha(q), \Phi_B)$ soft contribution, see eq. (A.7). This description applies to the physical case of *bare* muons, namely not clustered with surrounding photon radiation. For the case of electrons, a calorimetric definition in terms of *dressed* leptons is more appropriate from the experimental point of view. This would require an extension of our formalism to resum a new kind of observable, such as the dressed-lepton analogue of the q_T imbalance [149–153], and is left for future work.

The pure QED correction to the Sudakov radiator is then

$$R^{\text{QED}}(k_{t1}) = \int_{k_{t1}}^{M} \frac{\mathrm{d}q}{q} \left\{ \sum_{\ell=1}^{2} \left[A'_\ell(\alpha(q)) \ln \frac{M^2}{q^2} + B'_\ell(\alpha(q)) \right] + D'(\alpha(q), \Phi_B) \right\}, \qquad (2.11)$$

where ℓ ranges in $1, 2$, as is the case for QCD, since no collinear singularities are associated to massive leptons, i.e. the corresponding A'_ℓ and B'_ℓ functions are null. Up to NLL QED accuracy, eq. (2.11) can be cast as

$$R^{\text{QED}}(k_{t1}) = -L\, g'_1(\lambda') - g'_2(\lambda'), \qquad (2.12)$$

in terms of $\lambda' = \alpha\, \beta'_0\, L$, with β'_0 being the first coefficient of the QED beta function. The $g'_{1,2}(\lambda')$ functions are written in terms of the anomalous dimensions $A'^{(1)}_\ell$, $A'^{(2)}_\ell$, $B'^{(1)}_\ell$, and $D'^{(1)}(\Phi_B)$, whose expressions are collected in appendix A.

Genuine mixed QCD-EW contributions to the Sudakov radiator stem from QED (QCD) corrections to QCD (QED) running couplings, as well as from mixed $\mathcal{O}(\alpha_s^n \alpha^m)$ soft-collinear and hard-collinear anomalous dimensions, $A^{(n,m)}$ and $B^{(n,m)}$ respectively. We note that the $\mathcal{O}(\alpha_s \alpha)$ soft-collinear anomalous dimension $A^{(1,1)}$ is null, hence at NLL in the mixed expansion (terms of order $\alpha_s^n \alpha^m \ln(1/v)^{n+m}$) the correction to the radiator simply amounts to

$$R^{\text{MIX}}(k_{t1}) = -\frac{1}{2\pi} \sum_{\ell=1}^{2} \int_{k_{t1}}^{M} \frac{\mathrm{d}q}{q} \left[\frac{\alpha_s^2 \beta_{01} \ln \xi'}{\xi^2 \beta'_0} A_\ell^{(1)} + \frac{\alpha^2 \beta'_{01} \ln \xi}{\xi'^2 \beta_0} A_\ell'^{(1)} \right] \ln \frac{M^2}{q^2}, \qquad (2.13)$$

with $\xi = 1 - 2\alpha_s \beta_0 \ln \frac{\mu_R}{q}$, $\xi' = 1 - 2\alpha \beta'_0 \ln \frac{\mu_R}{q}$, and β_{01} (β'_{01}) representing the lowest-order QED (QCD) contribution to the QCD (QED) running, see also [101, 102]. The result can be written as

$$R^{\text{MIX}}(k_{t1}) = -g_{11}(\lambda, \lambda') - g'_{11}(\lambda, \lambda'), \qquad (2.14)$$

with constituent functions again given in appendix A.

Although the $B^{(1,1)}$ coefficient [56] enters at NNLL accuracy, as it generates terms of order $\alpha_s^n \alpha^m \ln(1/v)^{n+m-1}$, we nevertheless include it in the Sudakov exponent to correctly account for all single-logarithmic contributions of order $\alpha_s \alpha \ln(1/v)$. Our complete radiator including EW effects then reads

$$R(k_{t1}) = \left[R(k_{t1}) \right]_{\text{eq. (2.4)}} + R^{\text{QED}}(k_{t1}) + R^{\text{MIX}}(k_{t1}) + \frac{\alpha_s}{2\pi} \frac{\alpha}{2\pi} B^{(1,1)} L. \qquad (2.15)$$

We refer to NLL_{EW} accuracy when considering EW effects stemming from $R^{\text{QED}}(k_{t1}) + R^{\text{MIX}}(k_{t1})$ in eq. (2.15), and to nNLL_{MIX} accuracy when including $B^{(1,1)}$ as well. The

nomenclature suggests that such a term is of mixed QCD-EW origin, and is part of the NNLL correction in the mixed coupling expansion.

Turning now to the analysis of luminosity factor in eq. (2.5), its leading EW corrections amount to the following replacements:

$$C_{ab}(z) = \left[C_{ab}(z) \right]_{\text{eq. (2.6)}} + \frac{\alpha}{2\pi} C_{ab}'^{(1)}(z) + \frac{\alpha_s}{2\pi} \frac{\alpha}{2\pi} C_{ab}^{(1,1)}(z),$$

$$H(\mu_R) = \left[H(\mu_R) \right]_{\text{eq. (2.6)}} + \frac{\alpha}{2\pi} H'^{(1)}(\mu_R) + \frac{\alpha}{2\pi} F'^{(1)}(\Phi_B) + \frac{\alpha_s}{2\pi} \frac{\alpha}{2\pi} H^{(1,1)}(\mu_R). \quad (2.16)$$

In eq. (2.16), $C_{ab}'^{(1)}(z)$ and $F'^{(1)}(\Phi_B)$ refer to $\mathcal{O}(\alpha)$ QED constants of initial-state collinear and soft wide-angle origin, respectively, obtained abelianising the corresponding QCD expressions [99, 100, 148]. $H'^{(1)}(\mu_R)$ is the EW one-loop virtual correction, that we evaluate with RECOLA [154, 155]. The inclusion of primed quantities in eq. (2.16) allows one to reach NLL_{EW}' level, i.e. to correctly capture all terms of order $\alpha^n \ln(1/v)^{2n-2}$ in the cumulative cross section. Quantities labelled with "(1, 1)" in eq. (2.16) formally enter at order $\alpha_s^n \alpha^m \ln(1/v)^{n+m-2}$ in the cumulative cross section, thus they are beyond NLL' accuracy in both QCD and EW expansions. However, they need to be included if one aims at matching the resummed calculation with a fixed-order prediction at $\mathcal{O}(\alpha_s \alpha)$ accuracy. We define the accuracy attained by means of their inclusion as $\text{nNLL}_{\text{MIX}}'$, consistently with the nomenclature introduced above. Corresponding to the modifications detailed in eq. (2.16), DGLAP evolution is now ruled by

$$\hat{P}_{ij}(z) = \left[\hat{P}_{ij}(z) \right]_{\text{eq. (2.7)}} + \frac{\alpha}{2\pi} \hat{P}_{ij}'^{(1)}(z) + \frac{\alpha_s}{2\pi} \frac{\alpha}{2\pi} \hat{P}_{ij}^{(1,1)}(z), \quad (2.17)$$

in terms of the QED ($\hat{P}'^{(1)}$) and mixed QCD-QED ($\hat{P}^{(1,1)}$) splitting kernels reported in [99, 100].

A concluding remark on the inclusion of photon-initiated contributions is in order. A photon PDF in the luminosity $\mathcal{L}(k_{t1})$ is needed in the context of EW corrections to Drell Yan. This is due to the presence of $C_{q\gamma}'(z)$ coefficient functions in eq. (2.16), as well as to QED contributions to DGLAP evolution in eq. (2.17). Moreover, in the case of NCDY, a purely photon-induced Born channel $|\mathcal{M}_B|_{\gamma\gamma}^2$ is active. Although its impact on the fiducial cross section is at the percent level with respect to QCD corrections, see [63], its effects on differential distributions are not necessarily negligible with respect to the other EW corrections we include. In our simulations we consider all photon contributions mentioned above, and consistently adopt PDF sets that feature a photon density [156]. We instead refrain from including photon-initiated channels in the $\mathcal{O}(\alpha_s \alpha)$ constant contribution, as numerically negligible [63].

3 Validation

In this section we provide a validation of our implementation of EW effects in Drell Yan. We start by describing the physical setup we employ. We consider NCDY at the LHC, $pp \to Z/\gamma^* (\to \mu^+ \mu^-) + X$, with centre-of-mass energy $\sqrt{s} = 14 \, \text{TeV}$. For the EW couplings we use the G_μ scheme with $G_F = 1.1663787 \times 10^{-5} \, \text{GeV}^{-2}$ and set on-shell masses and widths to the values $m_{W,\text{OS}} = 80.385 \, \text{GeV}$, $m_{Z,\text{OS}} = 91.1876 \, \text{GeV}$, $\Gamma_{W,\text{OS}} = 2.085 \, \text{GeV}$,

and $\Gamma_{Z,\mathrm{OS}} = 2.4952\,\mathrm{GeV}$. Such mass values are converted to pole masses via the formula $m_V = m_{V,\mathrm{OS}}\,(1 + \Gamma_{V,\mathrm{OS}}^2/m_{V,\mathrm{OS}}^2)^{-1/2}$, with $V = W, Z$. The EW coupling is determined as $\alpha = \sqrt{2}\,G_F\,m_W^2\,(1 - m_W^2/m_Z^2)/\pi$, and the complex-mass scheme [157] is employed throughout. We consider massive muons, with $m_\mu = 105.658369\,\mathrm{MeV}$. Higgs and top-quark pole masses are set to $m_H = 125.9\,\mathrm{GeV}$ and $m_t = 173.07\,\mathrm{GeV}$, respectively. We use a diagonal CKM matrix. We assume $n_f = 5$ active quark flavours, and retain the exact m_t dependence in all virtual and real-virtual amplitudes associated to bottom-induced processes, except for the two-loop virtual corrections, where top-mass effects are neglected. We use the `NNPDF31_nnlo_as_0118_luxqed` PDF set [158], which is based on the LUXqed methodology [156] for the determination of the photon content of the proton. PDF sets are included through the `LHAPDF` interface [159]. DGLAP evolution, including the photon PDF, as well as convolutions with coefficient functions are performed by means of the `Hoppet` package [160]. All fixed-order predictions presented in the following, including those used for matching, are obtained with the MATRIX code [161]. More precisely, mixed QCD-EW corrections are validated against the calculations of refs. [60, 63].[1] Renormalisation and factorisation scales are set to $\mu_R = \mu_F = m^{\mu\mu}$, the di-muon invariant mass. To ensure a consistent matching between the RADISH and the MATRIX predictions, we set $\alpha(\mu_R) = \alpha|_{G_\mu}$, i.e. independent of the value of μ_R. The following selection cuts on the leptonic system are applied:

$$p_t^{\mu^\pm} > 25\,\mathrm{GeV}\,, \qquad |y^{\mu^\pm}| < 2.5\,, \qquad m^{\mu\mu} > 50\,\mathrm{GeV}\,, \tag{3.1}$$

with $p_t^{\mu^\pm}$ and $y^{\mu^\pm}$ the transverse momentum and rapidity of muons. Muons are considered at the bare (as opposed to dressed) level. The two-loop $\mathcal{O}(\alpha_s\alpha)$ corrections are calculated in the pole approximation [50, 52, 53, 60, 63]. This is based on a systematic expansion of the cross section around the heavy-boson resonance, in such a way that the radiative corrections are separated into well-defined, gauge-invariant contributions.

In order to detail our validation procedure, we introduce an additive matching of the resummation with the fixed-order prediction:

$$\frac{\mathrm{d}\sigma_{\mathrm{RES+FO}}}{\mathrm{d}p_t^{\mu\mu}} = \frac{\mathrm{d}\sigma_{\mathrm{RES}}}{\mathrm{d}p_t^{\mu\mu}} + \frac{\mathrm{d}\sigma_{\mathrm{FO}}}{\mathrm{d}p_t^{\mu\mu}} - \left[\frac{\mathrm{d}\sigma_{\mathrm{RES}}}{\mathrm{d}p_t^{\mu\mu}}\right]_{\mathrm{FO}}\,. \tag{3.2}$$

All contributions to the previous equation are differential cross sections with respect to the di-muon transverse momentum $p_t^{\mu\mu}$, as well as to all Born degrees of freedom Φ_B. The $\mathrm{d}\sigma_{\mathrm{RES}}$ term represents the resummed cross section detailed in section 2. In our case, the resummation is evaluated at $\mathrm{NLL}'_{\mathrm{EW}}$ ($\mathrm{nNLL}'_{\mathrm{MIX}}$) accuracy upon excluding (including) the terms labelled with "(1,1)" in eqs. (2.15) to (2.17). The $\mathrm{d}\sigma_{\mathrm{FO}}$ component is the fixed-order calculation for the DY process in presence of resolved radiation. Corresponding to a resummation at $\mathrm{NLL}'_{\mathrm{EW}}$ ($\mathrm{nNLL}'_{\mathrm{MIX}}$) accuracy, it includes corrections up to $\mathcal{O}(\alpha)$ ($\mathcal{O}(\alpha_s\alpha)$) with respect to Born level. Finally, $[\mathrm{d}\sigma_{\mathrm{RES}}]_{\mathrm{FO}}$ is the perturbative expansion of the resummed contribution $\mathrm{d}\sigma_{\mathrm{RES}}$, retaining the same order as featuring in $\mathrm{d}\sigma_{\mathrm{FO}}$, which removes the overlap between the two latter contributions.

Provided $\mathrm{d}\sigma_{\mathrm{RES}}$ in eq. (3.2) does *not* contain a resummation of subleading-power corrections through transverse-recoil effects [77, 89], the inclusive $p_t^{\mu\mu}$ integration of eq. (3.2)

---

[1]We thank the authors of refs. [60, 63] for providing us with a private version of MATRIX to perform the validation at $\mathcal{O}(\alpha_s\alpha)$.
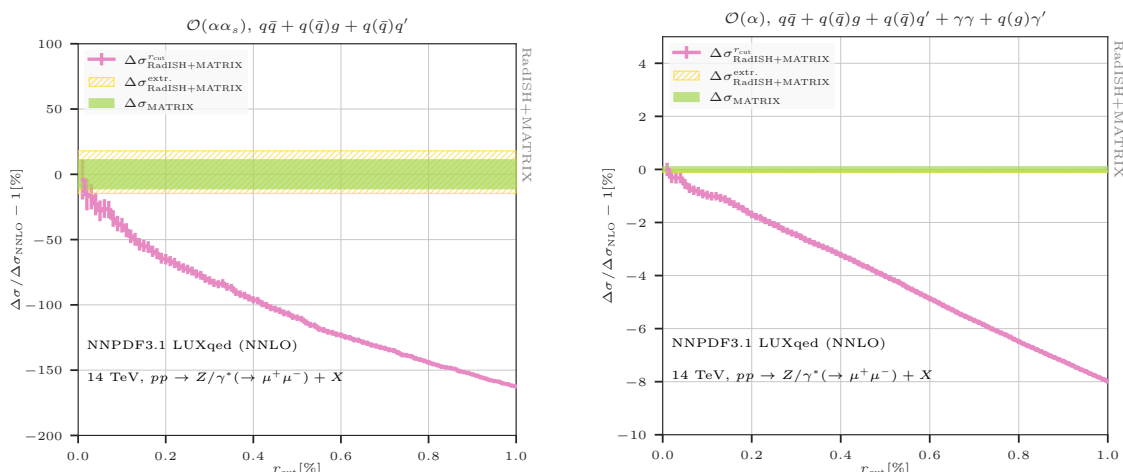
Figure 1. Fixed-order validation of the $\mathcal{O}(\alpha_s\alpha)$ (left panel) and $\mathcal{O}(\alpha)$ (right panel) contributions to the fiducial cross section.

yields the fixed-order cross section (differential in Φ_B) according to the q_T-subtraction formalism [162]. The main technical challenge in the implementation of eq. (3.2) is related to the fact that $d\sigma_{\mathrm{FO}}$ and $[d\sigma_{\mathrm{RES}}]_{\mathrm{FO}}$ are separately divergent in the small-$p_t^{\mu\mu}$ limit, and only their difference is integrable. This is typically handled by introducing a slicing parameter r_{cut} (or $p_{t,\mathrm{cut}}^{\mu\mu}$) and cutting off such a difference for $p_t^{\mu\mu}/m^{\mu\mu} < r_{\mathrm{cut}}$ (or $p_t^{\mu\mu} < p_{t,\mathrm{cut}}^{\mu\mu}$). The correct fixed-order rate is obtained ideally by taking the limit of slicing parameter going to 0, in practice by considering as small cut-off values as possible, compatibly with the numerical stability of the result.

In figure 1 we validate our implementation of eq. (3.2) at the level of fiducial cross section (i.e. inclusively integrated over $p_t^{\mu\mu}$), separately for the $\mathcal{O}(\alpha_s\alpha)$ contribution (left panel), and for the $\mathcal{O}(\alpha)$ contribution (right panel). The displayed results are summed over all contributing partonic channels, but validation plots of similar quality (except for the reduced statistics) have been produced for the individual channels. The pink bars are RADISH+MATRIX predictions as functions of r_{cut}, with bar widths representing the numerical integration error associated with the result. The RADISH+MATRIX label indicates that RADISH is responsible for the resummation components of eq. (3.2), while MATRIX provides the fixed order. The results labelled as MATRIX are based instead on an independent implementation of q_T subtraction. For consistency, the same fixed order component is used for the two predictions. The yellow band is an analytic extrapolation of the RADISH+MATRIX result to $r_{\mathrm{cut}} \to 0$, obtained by fitting the pink curve with a linear $p_t^{\mu\mu}$ function enhanced by logarithms of $p_t^{\mu\mu}$. The green reference band is the fixed-order correction to the fiducial cross section as obtained with MATRIX, and results are displayed as a relative difference with respect to the latter. The size of the extrapolation band is slightly different between the two computations, as it depends on the specific function used for the fit of the r_{cut} dependence, as well as on the r_{cut} range used in the extrapolation. The functions used in the RADISH+MATRIX predictions include the expected powers of logarithmically-enhanced contributions at $\mathcal{O}(\alpha_s\alpha)$ and $\mathcal{O}(\alpha)$, while MATRIX always adopts a quadratic function for its fit, and uses an optimised range to remove unstable points at the lowest values of r_{cut}.
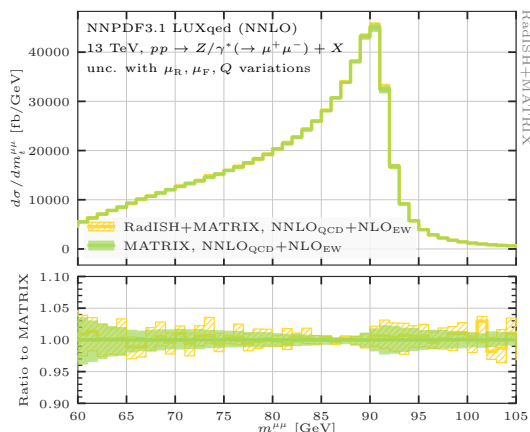
Figure 2. Fixed-order comparison of the RADISH+MATRIX implementation against MATRIX, differentially with respect to the di-muon transverse mass.

The uncertainty in the extrapolated value, which is 0.5 pb for MATRIX and 0.7 pb for RADISH, is in any case well below the scale uncertainty associated with the predictions, which is $\mathcal{O}(10)$ pb for the sole $\mathcal{O}(\alpha_s\alpha)$ correction.

Inspection of the two panels of figure 1 immediately reveals the computational challenges related to these calculations: large linear power corrections in $p_t^{\mu\mu}$ require extremely small values of $r_{\rm cut}$ for the q_T-subtracted prediction to become asymptotic, especially for the $\mathcal{O}(\alpha_s\alpha)$ correction. Such logarithmically-enhanced linear power corrections cannot be entirely reabsorbed via transverse recoil [77, 89], for instance using the procedure outlined in [163, 164], as they are in part caused by EW radiation [165] off the final-state leptons. For all coupling combinations we consider, the RADISH+MATRIX prediction correctly reproduces the MATRIX result in the asymptotic $r_{\rm cut} \to 0$ limit, within the respective numerical uncertainties. This represents a particularly powerful test for all aspects of the implementation. In particular, the logarithmic structure of the expanded cross section $[{\rm d}\sigma_{\rm RES}]_{\rm FO}$ is checked with high accuracy to reproduce the one of the fixed-order calculation ${\rm d}\sigma_{\rm FO}$, which is based on an independent numerical implementation. Moreover, a positive outcome of the plots in figure 1 also tests that the cumulative resummed prediction and its perturbative expansion coincide asymptotically in the $p_t^{\mu\mu} \to \infty$ limit. Although for the sake of clarity we show this behaviour only for $\mu_R = \mu_F = m^{\mu\mu}$ in figure 1, we have successfully tested it for all 7 uncorrelated μ_R and μ_F variations around the central choice.

In figure 2 we show the di-muon transverse-mass distribution at fixed order, including NNLO QCD (i.e. $\mathcal{O}(\alpha_s^2)$) and NLO EW (i.e. $\mathcal{O}(\alpha)$) corrections with respect to Born level, obtained both with RADISH+MATRIX (yellow) and with MATRIX (green). The transverse mass is defined as $m_t^{\mu\mu} = \left(2\,p_t^{\mu^+}\,p_t^{\mu^-}\,(1 - \cos\Delta\phi^{\mu\mu})\right)^{1/2}$, with $\Delta\phi^{\mu\mu}$ being the azimuthal separation of the two leptons. The plot is obtained with a slicing parameter $p_{t,{\rm cut}}^{\mu\mu} = 0.1\,{\rm GeV}$. It employs the same setup as detailed above, with the exception of the centre-of-mass energy, now set to $\sqrt{s} = 13\,{\rm TeV}$, and the selection cuts of eq. (3.1), which are replaced by the ATLAS cuts of ref. [14]:

$$p_t^{\mu^\pm} > 27\,{\rm GeV}\,, \qquad |\eta^{\mu^\pm}| < 2.5\,, \qquad 66\,{\rm GeV} < m^{\mu\mu} < 116\,{\rm GeV}\,. \tag{3.3}$$

In the whole $m_t^{\mu\mu}$ phase space, the RADISH+MATRIX fixed-order prediction is checked to precisely reproduce the MATRIX one both in shape and in normalisation. This holds for the central value of the prediction, as well as for the theoretical uncertainty band, obtained with a 7-point variation of μ_R and μ_F by factors of 2 around the common central value $m^{\mu\mu}$. The quality of the agreement is comparable across the entire $m_t^{\mu\mu}$ spectrum, namely both below and above the jacobian peak at $m_t^{\mu\mu} = m_Z$. As QCD and EW mechanisms have different relative importance in the various $m_t^{\mu\mu}$ regions, the successful comparison shown in figure 2 is a highly non-trivial test of their correct inclusion within our numerical framework. We stress that such a stringent differential test is possible only upon controlling the final-state leptons fully exclusively over their fiducial phase space, as our formalism in eq. (2.1) allows us to do.

4 Phenomenological results

For the phenomenological results of this section we consider both NCDY and CCDY at the 13 TeV LHC, in section 4.1 and section 4.2 respectively. The setup we use for NCDY is detailed at the beginning of section 3, with the fiducial cuts of eq. (3.3). In the case of CCDY, we consider the process $pp \to W^+(\to \mu^+\nu_\mu) + X$. Our choice for central μ_R and μ_F scales is $((m^{\mu\nu})^2 + (p_t^{\mu\nu})^2)^{1/2}$, with $m^{\mu\nu}$ ($p_t^{\mu\nu}$) the muon-neutrino invariant mass (transverse momentum). In the resummed calculation this expression is approximated with $m^{\mu\nu}$, which is correct up to quadratic power corrections in $p_t^{\mu\nu}$. The fiducial volume is defined by the following cuts on the charged lepton:

$$26\,\text{GeV} < p_t^{\mu^+} < 55\,\text{GeV}, \qquad |\eta^{\mu^+}| < 2.4, \qquad m_t^{\mu\nu} > 40\,\text{GeV}, \tag{4.1}$$

with $m_t^{\mu\nu} = \left(2\,p_t^{\mu^+} p_t^{\nu}(1 - \cos\Delta\phi^{\mu\nu})\right)^{1/2}$ the muon-neutrino transverse mass, and $\Delta\phi^{\mu\nu}$ the azimuthal separation between muon and neutrino.

All resummed predictions are obtained as detailed in section 2, with a modified version of the resummed logarithms [84, 166, 167] $L = \ln\left[(Q/k_{t1})^p + 1\right]/p$, with $p = 6$, in order to smoothly turn off logarithmic terms at $k_{t1} \gg Q$. The use of such logarithms, and consequently of a jacobian $J(k_{t1}) = dL/d\ln(Q/k_{t1})$ in the integration measure of eq. (2.1), induces a controlled set of p-dependent subleading power corrections in the formalism. Such terms do not affect the logarithmic accuracy of the calculation and, after matching, they exactly cancel up to the accuracy of the fixed-order component. Our results are obtained with the inclusion of transverse-recoil effects, which allow for the resummation of linear power corrections due to initial-state radiation [77, 89, 91].

We adopt the additive matching introduced in eq. (3.2) for all observables, except for the di-lepton transverse momentum $p_t^{\ell\ell}$ (equal to the di-muon transverse momentum $p_t^{\mu\mu}$ in NCDY, and to the muon-neutrino transverse momentum $p_t^{\mu\nu}$ in CCDY), where we consider a more general prescription [84, 91]:

$$\frac{d\sigma_{\text{RES+FO}}}{dp_t^{\ell\ell}} = \frac{d\sigma_{\text{FO}}}{dp_t^{\ell\ell}} + Z(p_t^{\ell\ell})\left\{\frac{d\sigma_{\text{RES}}}{dp_t^{\ell\ell}} - \left[\frac{d\sigma_{\text{RES}}}{dp_t^{\ell\ell}}\right]_{\text{FO}}\right\}, \tag{4.2}$$

with

$$Z(p_t^{\ell\ell}) = \left[1 - \left(p_t^{\ell\ell}/p_{t0}\right)^u\right]^h \Theta(p_{t0} - p_t^{\ell\ell}), \tag{4.3}$$

and $u = 2$, $h = 3$. The dampening profile $Z(p_t^{\ell\ell})$ ensures a smooth transition around the p_{t0} scale, from a soft regime $p_t^{\ell\ell} \ll p_{t0}$ in which the matched result must reduce to the resummed component, to a hard region $p_t^{\ell\ell} \gg p_{t0}$ where one must recover the fixed order. A choice of $Z(p_t^{\ell\ell}) \neq 1$ alters the unitarity of the matching (at the 1% level in our case), namely the $p_t^{\ell\ell}$ integral of eq. (4.2) does not reproduce the fixed-order result, hence it cannot be employed for q_T subtraction. Its use is however physically motivated for the $p_t^{\ell\ell}$ distribution, since the presence of the transition scale p_{t0} gives an extra handle to assess the matching systematics affecting the prediction. In the results presented below we vary p_{t0} in the range $\{2/3, 1, 3/2\} \times m_V$, with $m_V = m_Z$ (m_W) in NCDY (CCDY). The total uncertainty band assigned to matched predictions for the $p_t^{\ell\ell}$ distribution is the envelope of $9 \times 3 = 27$ variations, where 3 is the number of chosen values for p_{t0}, while 9 is the combination of the canonical 7 variations of μ_R, μ_F at central resummation scale $Q = m^{\ell\ell}/2$, with 2 variations of Q at central $\mu_R = \mu_F$.

In the following analysis our main focus is on the perturbative features of the new EW corrections, hence we don't include in our predictions a model for non-perturbative QCD corrections. Moreover, since currently there is no public implementation of the results of [60, 63, 64], the nNLL$'_{\mathrm{MIX}}$ predictions we present in the next sections do not contain mixed QCD-EW corrections to the fixed-order $\mathcal{O}(\alpha_s\alpha)$ component. We point out that, working at the level of bare muons, the inclusion of these terms can have a non-negligible impact on physical distributions such as the charged-lepton transverse momentum [53], since large logarithms of the muon mass enter the non-singular component $d\sigma_{\mathrm{FO}} - [d\sigma_{\mathrm{RES}}]_{\mathrm{FO}}$. These terms are expected to have a visible effect on sensitive observables such as the lepton transverse momentum, especially around the jacobian peak, where they can be as large as 10%, and may exceed the scale-uncertainty bands. We leave for future work a complete matching at this order, necessary for a thorough comparison with LHC data.

4.1 Neutral-current Drell Yan

We start by displaying in figure 3 the transverse momentum $p_t^{\mu\mu}$ of the di-muon system in NCDY. In the left panel we compare matched predictions with different accuracy. The purple band features NLO+NLL$'$ accuracy both in the QCD and in the EW coupling. We recall that this amounts to excluding all quantities with label "(1,1)" from eqs. (2.15) to (2.17). Green and orange bands both include nNLL$'_{\mathrm{MIX}}$ EW effects (i.e. "(1,1)" quantities in eqs. (2.15) to (2.17)), as well as NNLO$_{\mathrm{QCD}}$, with the orange (green) attaining N^{3}LL$'$ (NNLL$'$) logarithmic QCD accuracy. At medium-large $p_t^{\mu\mu}$ the inclusion of NNLO$_{\mathrm{QCD}}$ contributions has the effect of significantly hardening the tail, and reducing the uncertainty band to the 10–15% level. In the $p_t^{\mu\mu} \to 0$ resummation region, nNLL$'_{\mathrm{MIX}}$ and especially NNLL$'_{\mathrm{QCD}}$ logarithmic terms lower the spectrum (green vs purple), a trend which is maintained after inclusion of N^{3}LL$'_{\mathrm{QCD}}$ contributions (orange vs green). We notice that in this region the uncertainty band is significantly reduced upon adding logarithmic effects, down to the few-% level below 20 GeV for our most accurate prediction (orange). Predictions with higher formal accuracy are well contained within the uncertainty bands of lower orders in that region, which is a sign of good perturbative convergence.
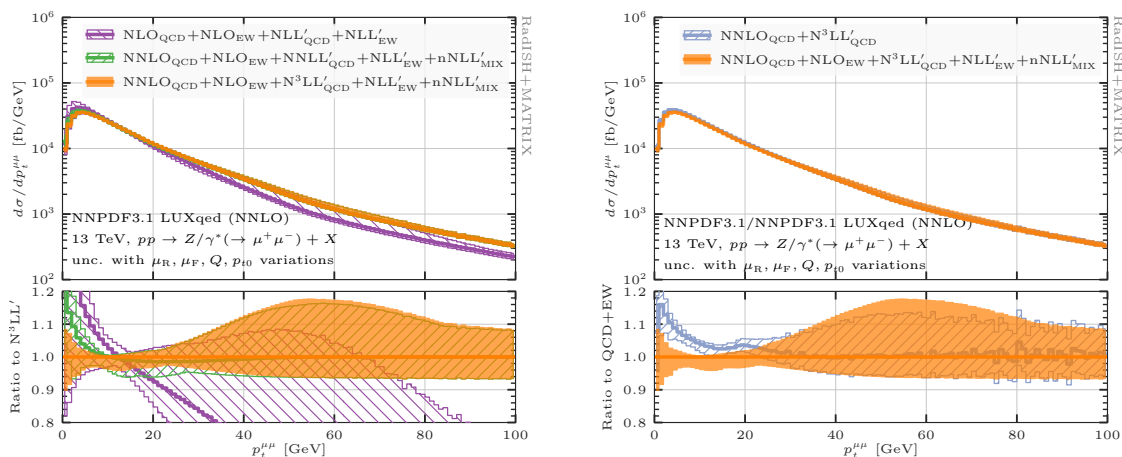
Figure 3. Matched spectra for the di-lepton transverse momentum in neutral-current DY. Left panel: perturbative progression including QCD and EW effects. Right panel: effect of EW corrections on top of the QCD baseline.

In the right panel of figure 3 we assess the importance of including EW effects (orange) on top of the QCD NNLO+N^{3}LL$'$ baseline (light blue). The orange band is identical to the one in the left panel, which will be the case as well for the next figures in this section. The two predictions differ by their perturbative content, as well as by the PDF adopted, where a LUXqed photon PDF (together with its DGLAP evolution) is active only for the former, whereas the latter is computed with the `NNPDF31_nnlo_as_0118` PDF set [168]. EW effects induce a visible distortion in the spectrum at small $p_t^{\mu\mu}$, lowering the prediction by as much as 10–15% for $p_t^{\mu\mu} \lesssim 10$ GeV. We have checked that, as one might expect, EW corrections largely factorise from QCD in the small-$p_t^{\mu\mu}$ region, namely similar shape distortions as those in the right panel of figure 3 can be observed when including EW effects on top of lower-order QCD predictions. The same considerations apply for all observables considered below. We also note that at small $p_t^{\mu\mu}$ the uncertainty bands of the two predictions are comparatively small, at the level of few %, and do not overlap. The latter feature is not surprising, since EW corrections are genuinely new physical effects, whose magnitude is not supposed to be meaningfully estimated by pure-QCD scale variations. This consideration highlights the relevance of an accurate description of EW effects in DY production for a successful precision-physics programme at the LHC. The effect of all-order EW corrections becomes more and more marginal for $p_t^{\mu\mu} \gtrsim 30$ GeV (except for a slight increase in the uncertainty band in the matching region), where the prediction starts being dominated by the fixed-order component. In this region one also expects that the inclusion of non-factorisable $\mathcal{O}(\alpha_s\alpha)$ QCD-EW effects, not considered in our results, may play a role.

In figure 4 we display differential predictions with respect to the transverse momentum $p_t^{\mu^+}$ of the positively charged muon. The inclusion of resummation effects is necessary to provide a physical description of this observable [169] due to its sensitivity to soft radiation for $p_t^{\mu^+} \simeq m^{\mu\mu}/2$. The pattern of the figure is identical to that of figure 3, with the perturbative progression displayed in the left panel, and the impact of EW effects in the right panel. At variance with the di-muon transverse momentum, the $p_t^{\mu^+}$ spectrum is non-trivial already at
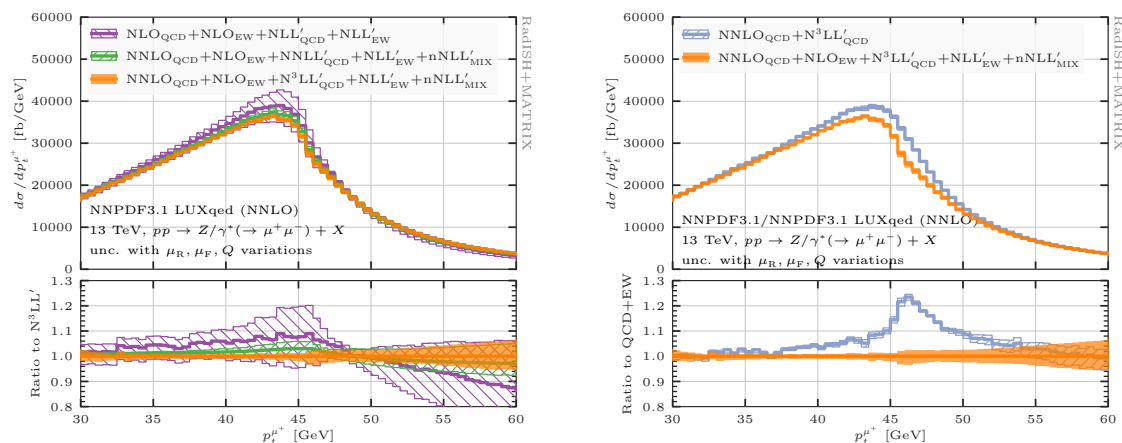
Figure 4. Matched spectra for the positively charged muon transverse momentum in neutral-current DY. Left panel: perturbative progression including QCD and EW effects. Right panel: effect of EW corrections on top of the QCD baseline.

Born level, hence we expect relatively milder perturbative corrections, and a solid perturbative stability across its entire phase space. This is what we find inspecting the left panel. Increasing QCD and EW formal accuracy (green vs purple) amounts to marginally lowering the jacobian peak and raising the tail at the level of roughly 5%. The inclusion of yet higher-order QCD resummation continues the trend, with a further few-% distortion. Theoretical uncertainty bands are found to reliably cover the central predictions of the next perturbative orders, both below and above the peak. The upgrade in formal accuracy has the visible effect of reducing the residual uncertainty, down to the level of $\pm 2\%$ ($\pm 4\%$) below (above) peak. As stated above, we expect however that a matching at $\mathcal{O}(\alpha_s \alpha)$, not included in our predictions, will have a numerical impact on the $p_t^{\mu^+}$ distribution. This may exceed the quoted perturbative uncertainty, especially around the jacobian peak, due to genuine mixed effects which are not captured by scale variations.

The right panel of figure 4 shows how the jacobian peak in $p_t^{\mu^+}$ is exposed to the interplay of QCD and EW effects. Including the latter has a clearly visible impact on the distribution, lowering the spectrum by as much as 20% at $p_t^{\mu^+} \simeq m_Z/2$, in a way that by no means can be approximated by a constant rescaling factor. The shape of the correction is compatible with what observed in [170] (see figure 24) in the context of a comparative study among event generators with QED resummation. In our case, the prediction including EW effects lies outside of the pure-QCD uncertainty band in the whole peak region, roughly from 35 GeV to 55 GeV. This accentuates what was observed in the right panel of figure 3 at small $p_t^{\mu\mu}$, highlighting the need for EW corrections for a complete description of this observable.

The di-muon transverse mass $m_t^{\mu\mu}$, displayed in figure 5, follows a similar pattern as the muon transverse momentum in figure 4. A solid perturbative convergence is observed in the left panel, both below and especially above the jacobian peak at $m_t^{\mu\mu} \simeq m_Z$. Perturbative corrections are relatively flat upon including EW effects, at the level of up to 5% comparing purple and orange predictions. Uncertainty bands are significantly shrunk by the inclusion of subleading perturbative effects, again reaching $\pm 2\%$ ($\pm 4\%$) below (above) peak. The right panel shows that EW effects have moderate impact below the transverse-mass peak,
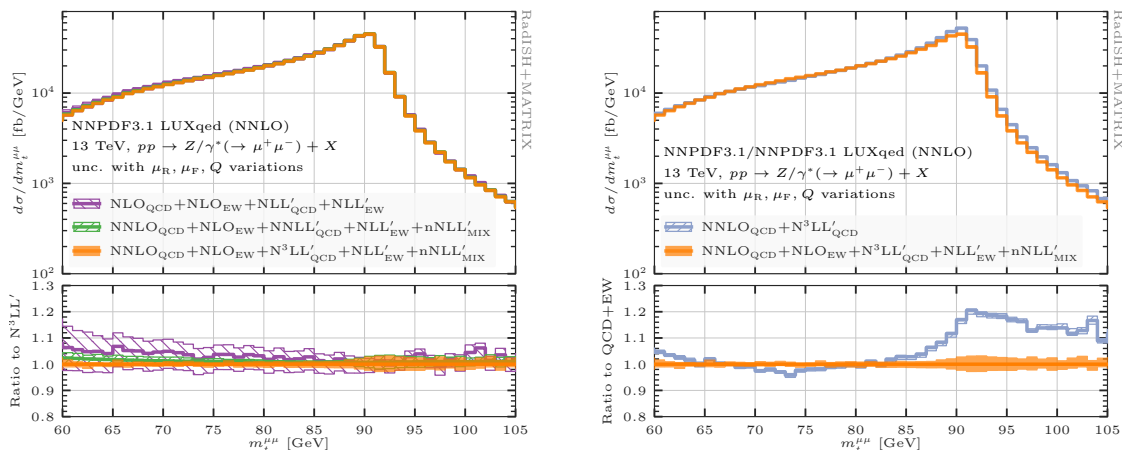
Figure 5. Matched spectra for the di-muon transverse mass in neutral-current DY. Left panel: perturbative progression including QCD and EW effects. Right panel: effect of EW corrections on top of the QCD baseline.

with shape distortions at the $\pm 3\%$ level for $m_t^{\mu\mu} \lesssim 85\,\mathrm{GeV}$. In the peak region and in the high-$m_t^{\mu\mu}$ tail the distortion reaches the 15–20% level, with EW contributions consistently lowering the prediction.

In figure 6 we show the same observables that were considered in figures 3 to 5, comparing RADISH+MATRIX predictions against POWHEG$_{\mathrm{QCD+EW}}$ [116, 117] results. The latter tool performs an NLO + parton shower (PS) matching including NLO QCD and NLO EW effects at the level of matrix elements, as well as the resummation of QED and QCD initial-state radiation (ISR) by means of PYTHIA8 [107] (version 8.245), and the resummation of QED final-state radiation (FSR) by means of PHOTOS [104]. In order for the comparison with RADISH+MATRIX to be sensible, we do not consider hadronisation and multi-parton interactions (MPI) at the end of the PYTHIA8 showering phase. We adopt the AZNLO tune [171], that was fit to precise Drell-Yan $p_t^{\ell\ell}$ and ϕ_η^* data. Moreover, we activate the POWHEG$_{\mathrm{QCD+EW}}$ flag `lepaslight=0`, in order to treat the final-state muons as massive. POWHEG$_{\mathrm{QCD+EW}}$ contains QCD and EW ingredients entering our NLO+NLL′ results.[2] As such, POWHEG$_{\mathrm{QCD+EW}}$ predictions (pink curves in figure 6) are expected to be fairly compatible with the RADISH+MATRIX ones at NLO+NLL′ accuracy (purple lines) within their respective uncertainties. Both are confronted to our best predictions (orange lines) to assess the numerical impact, with respect to the current state of the art, of the terms included in the present article for the first time. For clarity, we stress that the purple and orange RADISH+MATRIX predictions are the same (with identical colour code) as displayed in the left panels of figures 3 to 5.

Starting with the di-muon transverse momentum $p_t^{\mu\mu}$ in the upper-left panel of figure 6, we note that the RADISH+MATRIX (purple) and POWHEG$_{\mathrm{QCD+EW}}$ (pink) central predictions are in reasonable shape agreement in the resummation region $p_t^{\mu\mu} \lesssim 20\,\mathrm{GeV}$. As far as the hard $p_t^{\mu\mu}$ tail is concerned, we instead observe a different shape between the two

---

[2]We note that the photon-induced process $\gamma\gamma \to \mu^+\mu^-$ at LO is not available in the current version of the NCDY POWHEG$_{\mathrm{QCD+EW}}$ generator `Z_ew-BMNNPV` revision 4056.
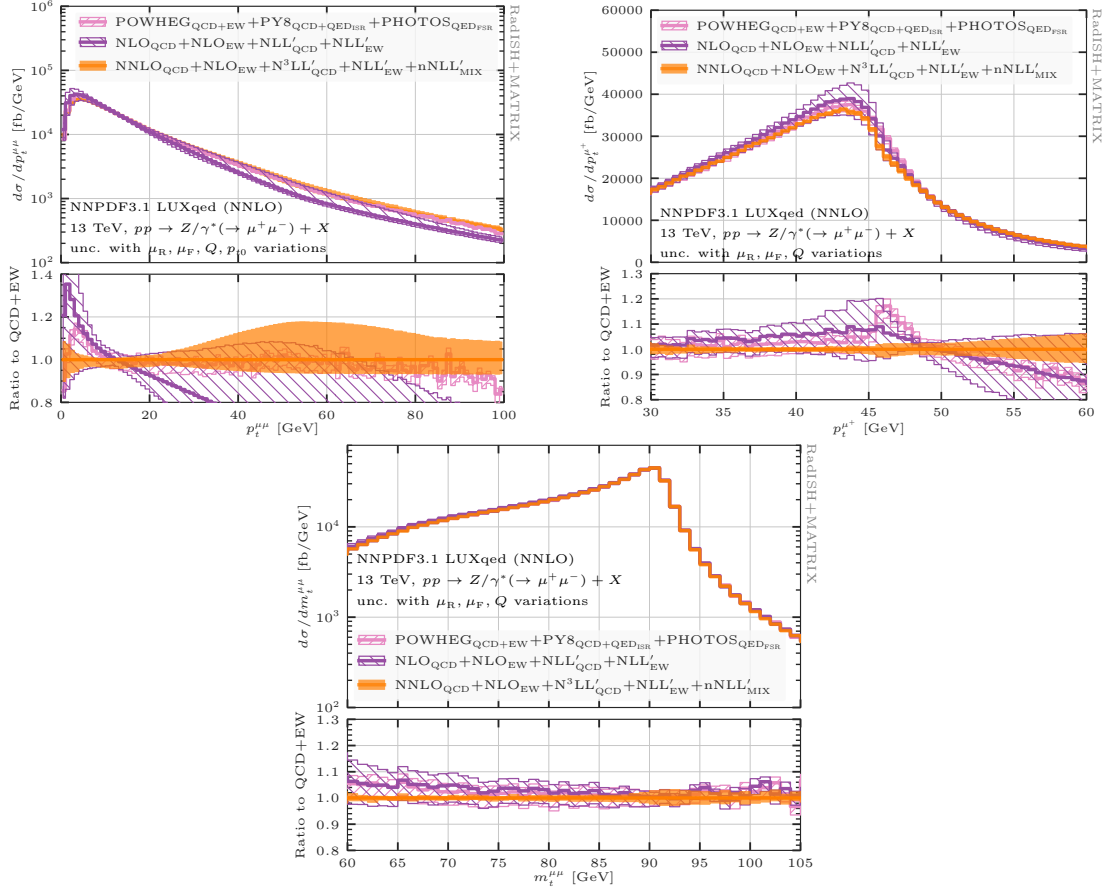
Figure 6. Comparison of matched RADISH+MATRIX spectra (purple and orange) against POWHEG$_{\text{QCD+EW}}$ predictions (pink) for the di-muon transverse momentum, the positively charged muon transverse momentum, and the di-muon transverse mass in neutral-current Drell Yan.

generators. We have checked that the RADISH+MATRIX result reproduces the fixed-order one from $p_t^{\mu\mu} \simeq 50\,\text{GeV}$ on. Conversely, the transition region between resummed and fixed-order regimes is shifted to larger transverse momenta and is broader in the POWHEG$_{\text{QCD+EW}}$ description. This behaviour is controlled by the parameters ruling the exponentiation of non-singular contributions in the POWHEG Sudakov form factor [172, 173], implemented through the POWHEG damping mechanism. The main criterion used to damp the non-singular regions is based on the departure of the real matrix element from its soft and/or collinear approximations. For the plots in figure 6 we adopt the POWHEG option `bornzerodamp=0`, enabling the exponentiation of the full NLO real matrix element. With this setting the POWHEG$_{\text{QCD+EW}}$ tail gets accidentally close to the orange RADISH+MATRIX curve for $50 \lesssim p_t^{\mu\mu} \lesssim 150\,\text{GeV}$, although not featuring any exact NNLO information contained in the latter, before reducing to the NLO result at larger $p_t^{\mu\mu}$. The matching systematics associated with the arbitrariness of the damping factor is not included in the POWHEG$_{\text{QCD+EW}}$ uncertainty, which is obtained with a standard 7-point variation of the μ_R and μ_F scales. The relative smallness of the quoted POWHEG$_{\text{QCD+EW}}$ band is then partially driven by missing information on resummation (Q) and matching (p_{t0}) uncertainties. Moreover, scale variations

in POWHEG$_{\text{QCD+EW}}$ have an effect only at the level of Les Houches events [174, 175], and are not entirely propagated in the showering phase. We stress that such a feature is rather common in NLO+PS computations, which typically do not include uncertainties stemming from the variations of μ_R and μ_F within the parton shower. A comparison of POWHEG$_{\text{QCD+EW}}$ with the most accurate RADISH+MATRIX prediction (pink vs orange) highlights the importance of including higher-order QCD and mixed QCD-EW effects. The shape modifications they induce with respect to the POWHEG$_{\text{QCD+EW}}$ state of the art significantly exceed the quoted uncertainty band for the latter, which is foreseen to have an impact on precision DY phenomenology.

Turning to the positively-charged muon transverse momentum $p_t^{\mu^+}$ in the upper-right panel of figure 6, we observe that the region around the jacobian peak at $p_t^{\mu^+} \simeq m_Z/2$ is fairly sensitive to multiple soft and collinear radiation, hence to resummation effects. The remarkable level of compatibility between RADISH+MATRIX and POWHEG$_{\text{QCD+EW}}$ results with similar physical content (purple vs pink curves, i.e. NLO+NLL′ in QCD and EW couplings) reflects the agreement of the two results at small $p_t^{\mu\mu}$, already noticed in the upper-left panel of figure 6. The conclusions drawn earlier for the comparison with the best RADISH+MATRIX result (pink vs orange) apply for $p_t^{\mu^+}$ as well, with shape distortions up to $\pm 15\%$ in the displayed range, and a significant reduction of theoretical uncertainty after inclusion of higher-order corrections.

The di-muon transverse mass $m_t^{\mu\mu}$ shown in the lower panel of figure 6 follows the same pattern, with a good agreement of central predictions from POWHEG$_{\text{QCD+EW}}$ and RADISH+MATRIX (pink vs purple) at NLO+NLL′ accuracy. Shape distortions induced by higher-order contributions (pink vs orange) are milder than for $p_t^{\mu^+}$, and solely concern the region below the jacobian peak, almost reaching -10% in the displayed range. The reduction of theoretical uncertainty is again consistent, across the entire range, and more than a factor of 2 at small $m_t^{\mu\mu}$.

4.2 Charged-current Drell Yan

We now turn to predictions for CCDY at the LHC, starting in figure 7 with the muon-neutrino transverse momentum $p_t^{\mu\nu}$. Given the similarity of this observable with $p_t^{\mu\mu}$ in NCDY, the pattern displayed in figure 7 is fairly similar qualitatively to that in figure 3. From the left panel, we just remark a slightly larger residual uncertainty band with respect to NCDY, reaching the 25% level in the matching region for our best prediction (orange) at $p_t^{\mu\nu} \simeq 50\,\text{GeV}$. In the resummation region the uncertainty decreases to the few-% level, showing clear perturbative convergence. In the right panel, the inclusion of EW corrections is again responsible for lowering the spectrum with respect to the QCD baseline below 20 GeV. In this case, the effect is quantitatively smaller than for NCDY, at the level of 5–10% at most, compatibly with the presence of a single (as opposed to two) source of QED radiation in the CCDY Born final state.

Figures 8 and 9 show predictions for the muon transverse momentum $p_t^{\mu^+}$ and for the muon-neutrino transverse mass $m_t^{\mu\nu}$. These distributions are central for the determination of fundamental SM parameters such as the W-boson mass, serving as inputs for template-fitting techniques [1–5], or for the definition of new observables [120, 121] based on their perturbative
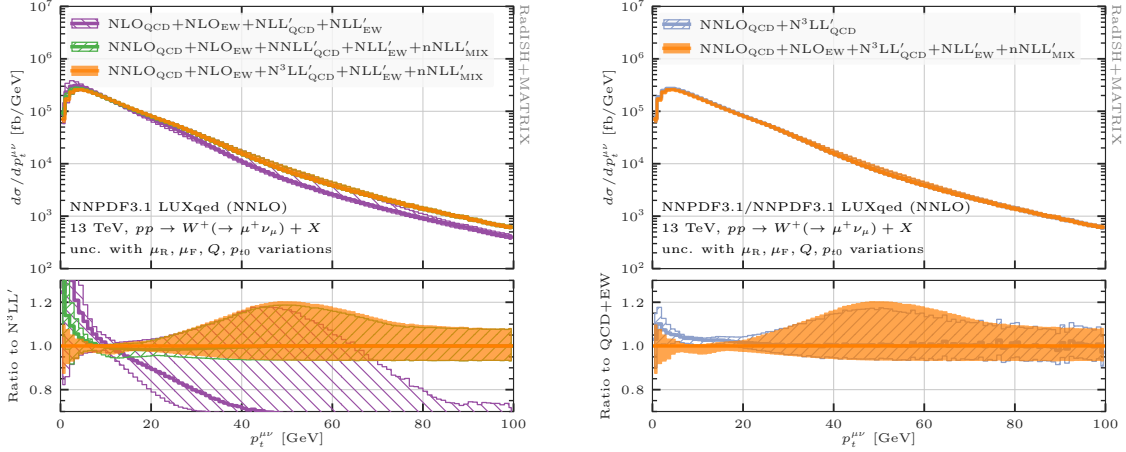
Figure 7. Matched spectra for the muon-neutrino transverse momentum in charged-current DY. Left panel: perturbative progression including QCD and EW effects. Right panel: effect of EW corrections on top of the QCD baseline.
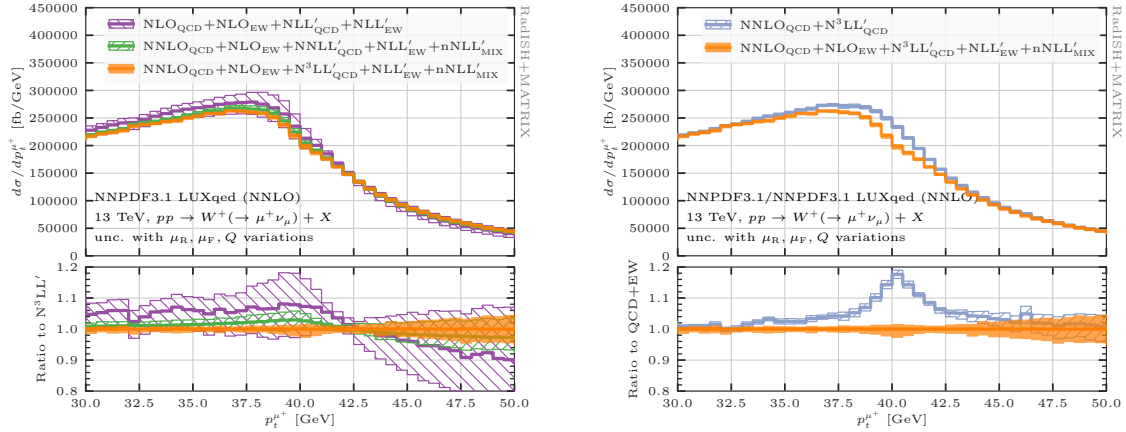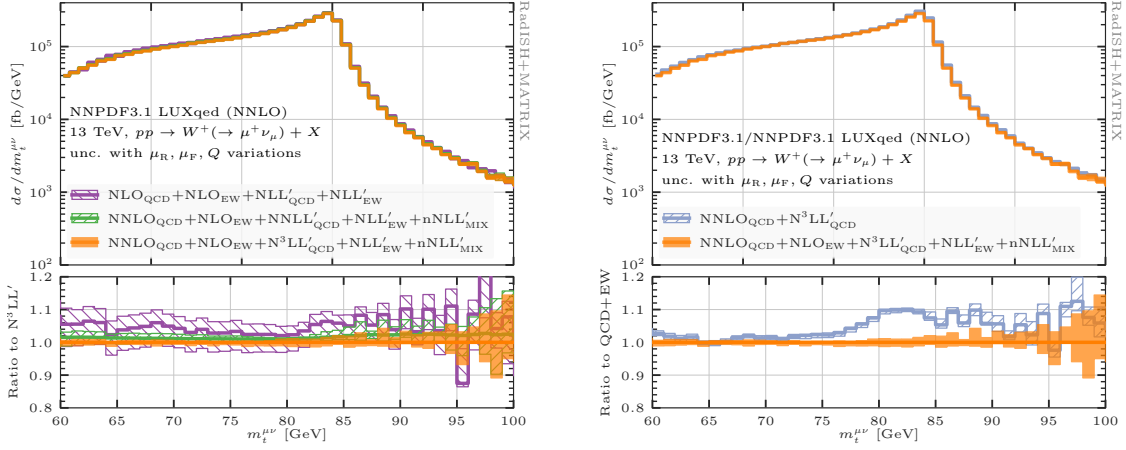

Figure 8. Matched spectra for the muon transverse momentum in charged-current DY. Left panel: perturbative progression including QCD and EW effects. Right panel: effect of EW corrections on top of the QCD baseline.

prediction. By and large, the same comments expressed for the analogous NCDY observables apply in CCDY as well, with a remarkable perturbative stability displayed by all predictions including EW effects (left panels of figures 8 and 9), and visible shape distortions induced by the latter on top of pure-QCD predictions (right panels of figures 8 and 9). From the quantitative point of view, the effect of EW corrections is slightly smaller than for NCDY, consistently with what noticed for $p_t^{\mu\nu}$ in the right panel of figure 7. The trend is also very similar to what found in figure 24 of [170], both for $p_t^{\mu^+}$ and for $m_t^{\mu\nu}$.

As for the comparison with POWHEG$_{\text{QCD+EW}}$ in CCDY, in figure 10 we show predictions for the muon-neutrino transverse momentum, the muon transverse momentum, and the muon-neutrino transverse mass, with the same pattern used in figure 6. The features of the comparison are very similar, both qualitatively and quantitatively, to the ones already exposed in detail for NCDY, thus we refrain from further commenting on them. Given

Figure 9. Matched spectra for the muon-neutrino transverse mass in charged-current DY. Left panel: perturbative progression including QCD and EW effects. Right panel: effect of EW corrections on top of the QCD baseline.
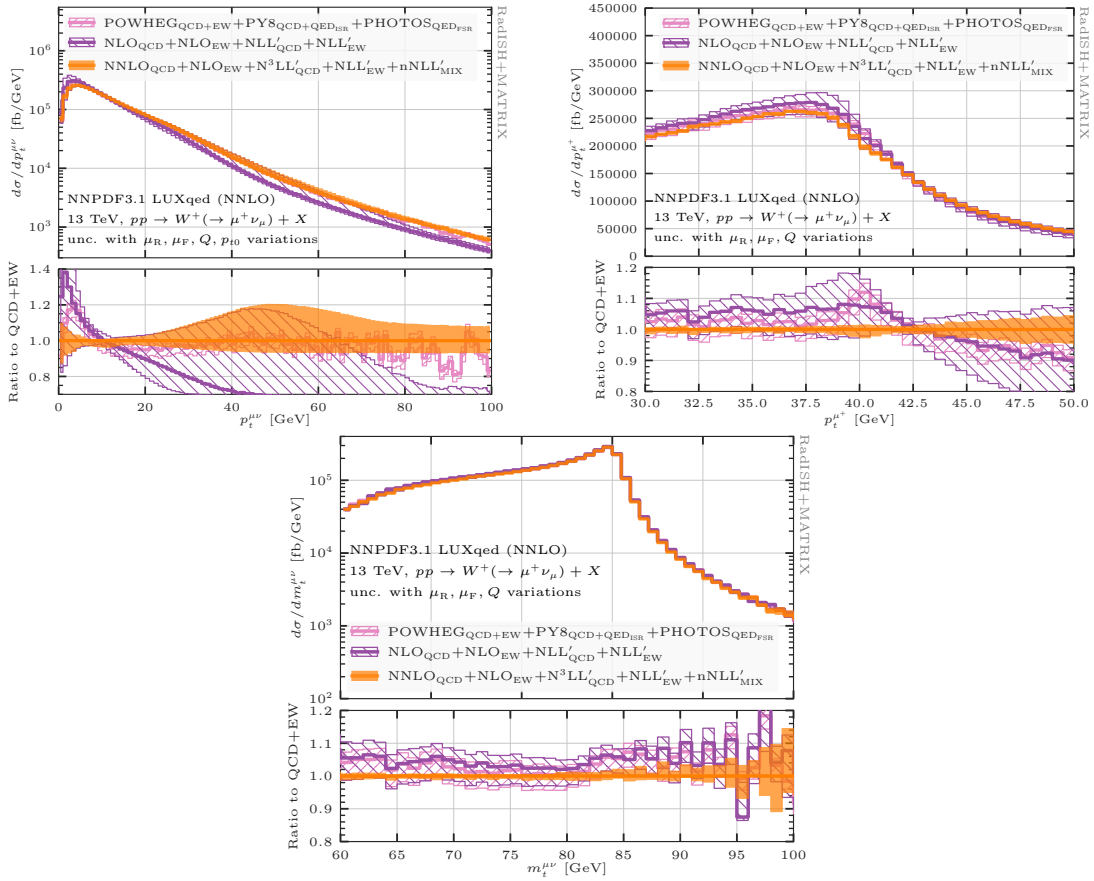
Figure 10. Comparison of matched RadISH+MATRIX spectra (purple and orange) against POWHEG$_{\mathrm{QCD+EW}}$ predictions (pink) for the muon-neutrino transverse momentum, the muon transverse momentum, and the muon-neutrino transverse mass in charged-current Drell Yan.
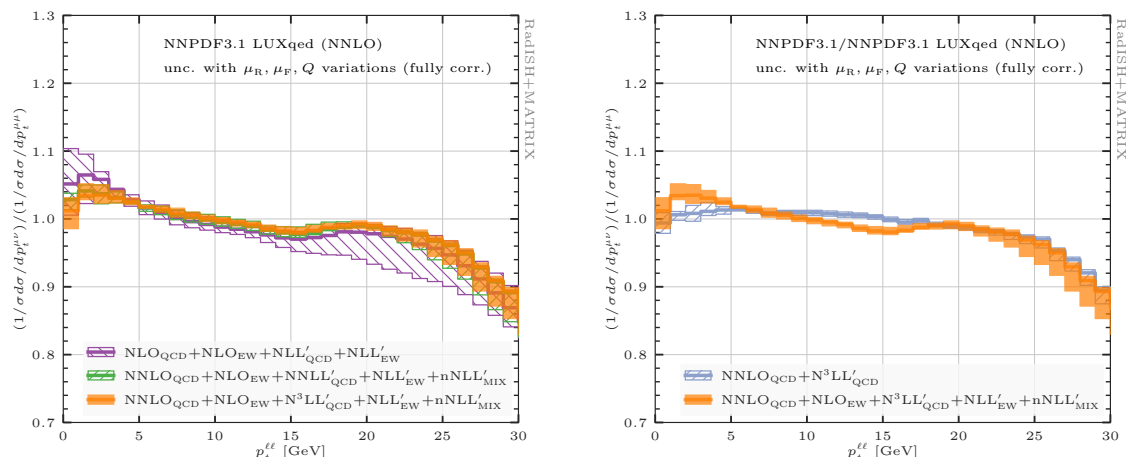
Figure 11. Normalised ratio of charged- to neutral-current Drell Yan di-lepton transverse momentum. Variations of μ_R, μ_F, and Q are correlated between the numerator and the denominator of the ratio. Left panel: perturbative progression including QCD and EW effects. Right panel: effect of EW corrections on top of the QCD baseline.

the high phenomenological relevance for these observables, we are confident that our new RADISH+MATRIX predictions with highest accuracy (orange curves) will have an impact on the precise determination of the W-boson mass and the EW mixing angle at the LHC.

4.3 Comparison between neutral- and charged-current Drell Yan

We conclude the section of phenomenological results by showing the normalised ratio of the CCDY to NCDY di-lepton transverse momentum $p_t^{\ell\ell}$. This is a crucial control observable in the experimental strategy for W-boson mass extraction at the LHC [2]. The differential spectra are normalised to the fiducial cross sections in the range $p_t^{\ell\ell} \in [0, 30]\,\text{GeV}$.

In figure 11, using the same pattern as in the previous figures, we display RADISH+MATRIX predictions for the ratio observable. We do not consider variations of the matching scheme, i.e. we set $Z(p_t^{\ell\ell}) = 1$ in eq. (4.2). Uncertainty bands are obtained with a fully correlated variation of the three perturbative scales μ_R, μ_F, and Q in the numerator and in the denominator. From the left panel of figure 11 we observe a robust perturbative progression in presence of EW effects, with higher-order corrections stably contained into uncertainty bands of lower orders. There is a significant uncertainty reduction (green vs purple) upon inclusion of NNLO+NNLL′ QCD corrections and nNLL′$_{\text{MIX}}$ effects, while the further addition of N³LL′ QCD resummation (orange vs green) yields a more marginal reduction, essentially confirming the shape obtained at the previous QCD logarithmic accuracy. The shape itself is relatively non-trivial, as due to the interplay of EW corrections from initial- and final-state radiation with the fiducial cuts adopted. The right panel of figure 11 shows the impact of EW corrections (orange) on top of the QCD baseline (light blue). The main distortion is observed at small $p_t^{\ell\ell}$, compatibly with what was noticed in the individual di-lepton transverse momentum spectra in figure 3 and figure 7. EW effects increase the slope of the ratio at $p_t^{\ell\ell} \lesssim 15\,\text{GeV}$, reaching the level of $\pm 3\%$, and exceeding the QCD theoretical uncertainty band. We note that the impact of EW corrections on the ratio observable is
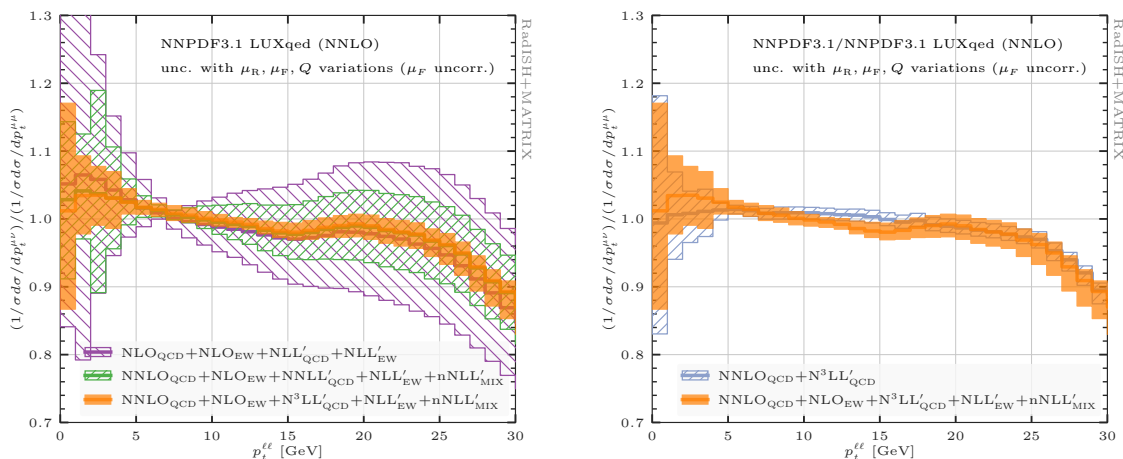
Figure 12. Normalised ratio of charged- to neutral-current Drell Yan di-lepton transverse momentum. Variations of μ_R, and Q are correlated between the numerator and the denominator of the ratio, while variations of μ_F are only constrained by $1/2 \leq \mu_F^{\text{num}}/\mu_F^{\text{den}} \leq 2$. Left panel: perturbative progression including QCD and EW effects. Right panel: effect of EW corrections on top of the QCD baseline.

significantly more pronounced than the $\pm 0.5\%$ observed in figure 6 of [103]. Apart from differences in the setup and in the perturbative accuracy, the bulk of the discrepancy is due to fact that the analysis of [103] is performed with undecayed Z and W gauge bosons, and inclusively over their phase space. We have checked that the ratio with EW effects indeed gets much closer to the pure QCD result upon removing the effect of QED radiation off final-state leptons. This highlights once more the importance of working with leptons at the fiducial level for precision DY phenomenology.

In figure 12 the CCDY to NCDY ratio is shown with a more conservative assumption on the correlation of scale variations. In particular, while the renormalisation and resummation scales are still varied in a fully correlated fashion, the factorisation scales for the numerator (μ_F^{num}) and for the denominator (μ_F^{den}) are varied independently, with the sole constraint $1/2 \leq \mu_F^{\text{num}}/\mu_F^{\text{den}} \leq 2$. This uncertainty prescription was already introduced in [86, 176], and is physically motivated by considering that CCDY and NCDY probe different combinations of partonic channels, and of PDFs in turn, hence full μ_F correlation may not be clearly justified. Decorrelating μ_F variations causes a significant inflation in uncertainty bands, especially at small $p_t^{\ell\ell}$ and for predictions with lower formal accuracy, as seen comparing the left panels of figure 12 and of figure 11. As a result of this more conservative uncertainty estimate, predictions with and without EW effects in the right panel of figure 12 are now marginally compatible.

Finally, figure 13 reports the comparison of RADISH+MATRIX and POWHEG predictions for the ratio observable, including QCD and EW contributions (left panel), or solely QCD effects (right panel). Although the POWHEG$_{\text{QCD+EW}}$ predictions for individual $p_t^{\ell\ell}$ distributions are in reasonable agreement with the NLO+NLL′ RADISH+MATRIX ones, the left panel of figure 13 reveals a moderate shape discrepancy in the ratio (purple vs pink), with POWHEG$_{\text{QCD+EW}}$ being steeper in the displayed range. The discrepancy is not covered assuming fully correlated uncertainties, and only upon decorrelating uncertainties
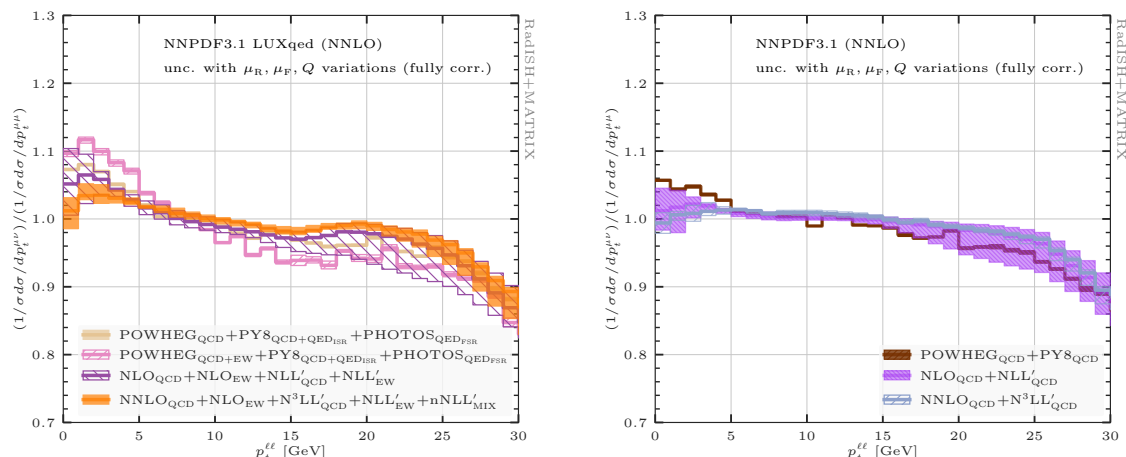
Figure 13. Comparison between RADISH+MATRIX and POWHEG for the normalised charged-to neutral-current Drell Yan di-lepton transverse momentum. Fully correlated variations of μ_R, μ_F, and Q are considered. Left panel: predictions including QCD as well as EW effects. Right panel: predictions including solely QCD effects.

do the two predictions become compatible with each other, due to the large uncertainty of the purple band in figure 12. As for the comparison of POWHEG$_{QCD+EW}$ with our most accurate predictions (pink vs orange), scale decorrelation is not sufficient to cover the difference between the two curves across the whole range. To further investigate this discrepancy, in the left panel of figure 13 we show in light brown a second POWHEG prediction, where QCD and QED showers are applied to a pure-QCD NLO sample obtained with the event generator of ref. [177]. The behaviour in this case is in good agreement with the RADISH+MATRIX NLO+NLL′ prediction (light brown vs purple). The effect caused by NLO EW matrix elements in POWHEG$_{QCD+EW}$ warrants further investigation, which however is beyond the scope of this article.

The POWHEG vs RADISH+MATRIX pattern at the level of pure QCD, displayed in the right panel of figure 13, is relatively similar to the light brown vs purple comparison in the left panel. The POWHEG prediction (dark brown) is slightly steeper, but still largely contained in the RADISH+MATRIX NLO+NLL′ correlated uncertainty band (lilac). Although we did not perform a detailed study, we have checked that the POWHEG prediction for the ratio is relatively insensitive to the employed PYTHIA8 tune, as well as to the inclusion of MPI and hadronisation effects, which hints at a perturbative explanation for the remaining differences. These shape features are qualitatively similar to the pattern observed in ref. [20], where a comparison for the ratio observable between POWHEG and RADISH can be deduced. There, POWHEG is found to describe data slightly better than RADISH, despite its substantially lower formal accuracy. However, we note that in ref. [20] the dominant effect of EW final-state radiation has been subtracted from the data, which moreover do not include any photon-induced contribution. The predictions presented in this article would allow for an accurate comparison including all sources of EW effects at the level of bare muons, as well as to establish more robustly the reliability of the EW subtraction procedure widely adopted in experimental analyses.

5 Conclusion

In this article we have presented an extension of the RADISH resummation framework to include dominant classes of QED, virtual EW and mixed QCD-EW effects in neutral- and charged-current Drell Yan lepton-pair production featuring massive bare leptons. Our predictions reach next-to-leading-logarithmic accuracy in the mixed QCD-EW coupling expansion, namely they correctly incorporate all contributions of order $\alpha_s^n \alpha^m L^{n+m}$, in terms of the QCD and EW coupling constants α_s and α, and of the large resummed logarithms L. They also include all terms, beyond next-to-leading logarithms, necessary to perform a consistent matching with fixed-order predictions at order $\mathcal{O}(\alpha_s \alpha)$ relative to the Born level, a development that we leave for future work.

The predictions presented here extend in several directions the current state of the art [102, 103] for the analytic resummation of mixed QCD-EW effects in Drell Yan. First, our resummation features further subleading terms with respect to those considered in [102, 103], in particular all contributions with a "(1,1)" label in eqs. (2.15) to (2.17), necessary for matching at order $\alpha_s \alpha$. Second, the resummation formalism is not limited to the di-lepton transverse momentum, but can be applied with no modifications to all observables resummed by RADISH, a notable example being ϕ_η^* in neutral-current Drell Yan. This can also open the door to the exploration of EW effects in different resummation environments still available in RADISH, such as jet-vetos or double-differential resummations, or for other scattering processes. Third, and most important, our predictions are fully differential in the phase space of the Drell Yan final-state leptons. Working with the leptonic final state enables a consistent account of off-shell and interference effects, as well as the inclusion of non-resonant channels, such as the photon-initiated Born contribution in neutral-current Drell Yan. Moreover, it enables a physical description of final-state QED photon radiation, which in our results is included both in charge- and in neutral-current Drell Yan. Being fully differential allows us to obtain predictions for leptonic Drell Yan observables of phenomenological interest, as well as to apply fiducial selection cuts to match experimental analyses. These features give our framework a level of flexibility comparable to the one of dedicated EW Monte Carlo generators [104–106, 116, 117], with the advantage of retaining a higher formal accuracy in the all-order resummation. We expect our predictions to have a direct impact on high-precision Drell Yan phenomenology, especially for the determination of fundamental Standard Model parameters such as the W-boson mass and the EW mixing angle.

We have displayed the impact of EW effects on physical distributions in neutral- and charged-current Drell Yan at the 13 TeV LHC. The perturbative behaviour is robust for all predictions including EW effects. Scale uncertainties affecting our most accurate QCD-EW results are at the level of 2–5% for inclusive observables such as the charged-lepton transverse momentum and the di-lepton transverse mass. The di-lepton transverse momentum has instead uncertainties that range from few-% in the resummation region, to 15–20% in the region where the transition to the fixed-order regime takes place.

We have been able to perform a meaningful comparison with EW Monte Carlo tools available in the literature. To this aim, we have used POWHEG$_{\text{QCD+EW}}$ [116, 117], which is the current state of the art for the resummation of the dominant QED effects in Drell Yan at leptonic level, and is used in Drell Yan experimental analyses. As for our NLO+NLL$'$ QCD and

EW predictions, the shape agreement with POWHEG$_{\text{QCD+EW}}$ is overall good, however we have argued that our estimate of theoretical uncertainties is more robust. Higher-order QCD and EW effects included in our predictions result in shape distortions in the resummation-dominated kinematical regions, which may in turn impact precision Drell Yan phenomenology.

In conclusion, accounting for EW effects on top of pure-QCD predictions causes modifications in the physical distributions that often exceed the quoted QCD theoretical uncertainty. This is for instance visible at small di-lepton transverse momentum, and around the jacobian peaks of the charged-lepton transverse momentum and of the transverse mass, with effects reaching 15–20%. This consideration highlights the importance of a complete description of Standard Model effects, not limited to QCD, for a successful precision-physics programme with Drell Yan observables at hadron colliders.

Acknowledgments

A Formulæ

In this section we report analytic elements relevant to the formulæ used in the main text.

The QCD beta function reads

$$\frac{\mathrm{d}\alpha_s(\mu)}{\mathrm{d}\ln\mu^2} = \beta(\alpha_s, \alpha) \equiv -\alpha_s\left(\beta_0\,\alpha_s + \beta_1\,\alpha_s^2 + \beta_{01}\,\alpha + \dots\right), \tag{A.1}$$

whose first two coefficients (with n_f active flavours, $C_A = N_c$, $C_F = \frac{N_c^2-1}{2\,N_c}$, and $N_c = 3$) are

$$\beta_0 = \frac{11\,C_A - 2\,n_f}{12\,\pi}, \qquad \beta_1 = \frac{17\,C_A^2 - 5\,C_A\,n_f - 3\,C_F\,n_f}{24\,\pi^2}. \tag{A.2}$$

Next we report the functions entering the QCD Sudakov radiator up to NLL, with $\lambda = \alpha_s(\mu_R)\,\beta_0\,L$, and $L = \ln\frac{Q}{k_{t1}}$. For Drell Yan, they read

$$g_1(\lambda) = \frac{A^{(1)}}{2\pi\beta_0}\frac{2\lambda + \ln(1-2\lambda)}{2\lambda},$$

$$\begin{aligned}
g_2(\lambda) = {} & \frac{A^{(1)}\ln\frac{M^2}{Q^2} + B^{(1)}}{4\pi\beta_0}\ln(1-2\lambda) - \frac{A^{(2)}}{8\pi^2\beta_0^2}\frac{2\lambda + (1-2\lambda)\ln(1-2\lambda)}{1-2\lambda} \\
& - \frac{A^{(1)}\beta_1}{8\pi\beta_0^3}\frac{\ln(1-2\lambda)\big[(2\lambda-1)\ln(1-2\lambda)-2\big] - 4\lambda}{1-2\lambda} \\
& - \frac{A^{(1)}}{4\pi\beta_0}\frac{2\lambda\big[1-\ln(1-2\lambda)\big] + \ln(1-2\lambda)}{1-2\lambda}\ln\frac{\mu_R^2}{Q^2},
\end{aligned} \tag{A.3}$$

with

$$A^{(k)} = \sum_{\ell=1}^{2} A_\ell^{(k)} = 2\,A_q^{(k)}\,, \quad B^{(1)} = \sum_{\ell=1}^{2} B_\ell^{(1)} = 2\,B_q^{(1)}\,,$$

$$A_q^{(1)} = 2\,C_F\,, \qquad\qquad A_q^{(2)} = 2\,C_F\left[C_A\left(\frac{67}{18} - \frac{\pi^2}{6}\right) - \frac{5}{9}\,n_f\right]\,, \quad B_q^{(1)} = -3\,C_F\,. \quad \text{(A.4)}$$

The EW beta function reads

$$\frac{\mathrm{d}\alpha(\mu)}{\mathrm{d}\ln\mu^2} = \beta'(\alpha, \alpha_s) \equiv -\alpha\left(\beta_0'\,\alpha + \beta_1'\,\alpha^2 + \beta_{01}'\,\alpha_s + \dots\right)\,, \quad \text{(A.5)}$$

with

$$\beta_0' = -\frac{N^{(2)}}{3\,\pi}\,, \qquad \beta_1' = -\frac{N^{(4)}}{4\,\pi^2}\,, \qquad N^{(k)} = N_c \sum_{q=1}^{n_f} e_{f_q}^k + \sum_{l=1}^{n_l} e_{f_l}^k\,, \quad \text{(A.6)}$$

with $f_q = q$ and $f_l = 2l + 9$ indicating quark and lepton flavours (following PDG conventions [178]), e_{f_q} being quark electric charges ($+2/3$ for up-type, $-1/3$ for down type), $e_{f_l} = -1$ being lepton charges, and n_l the number of lepton families considered.

The building blocks $g'_{1,2}(\lambda')$ of the NLL EW Sudakov radiator are obtained from the corresponding QCD functions in eq. (A.3) with the formal replacements $\lambda \to \lambda' = \alpha(\mu_R)\,\beta_0'\,L$, $\beta_k \to \beta_k'$, $A^{(k)} \to A'^{(k)}$, and $B^{(1)} \to \widetilde{B}'^{(1)}$. The relevant anomalous dimensions for Drell Yan are

$$A'^{(k)} = \sum_{\ell=1}^{2} A_\ell'^{(k)}\,, \qquad \widetilde{B}'^{(1)} = \sum_{\ell=1}^{2} B_\ell'^{(1)} + D'^{(1)}(\Phi_B)\,, \quad \text{(A.7)}$$

with [56, 60, 102, 165]

$$A_\ell'^{(1)} = 2\,e_{f(\ell)}^2\,, \qquad A_\ell'^{(2)} = -\frac{20}{9}\,N^{(2)}\,e_{f(\ell)}^2\,, \qquad B_\ell'^{(1)} = -3\,e_{f(\ell)}^2\,, \quad \text{(A.8)}$$

$$D'^{(1)}(\Phi_B) = -2\left[e_{f(3)}e_{f(4)}\frac{1+\beta^2}{\beta}\ln\frac{1+\beta}{1-\beta} + \sum_{\ell=1}^{2}\sum_{k=3}^{4}\left(\frac{e_{f(k)}^2}{2} + e_{f(\ell)}e_{f(k)}\ln\frac{s_{\ell k}^2}{s_{12}\,m^2}\right)\right]\,,$$

$f(j)$ the flavour of leg j, $s_{ij} = 2p_i\cdot p_j$, $\beta = \sqrt{1 - 4\,m^2/s_{12}}$, and m the mass of the charged final-state lepton(s).

The $\mathcal{O}(\alpha)$ soft wide-angle contribution reads [148, 179]

$$F'^{(1)}(\Phi_B) = \left(e_{f(3)}^2 + e_{f(4)}^2\right)\ln\frac{m_t^2}{m^2} + (e_{f(3)} + e_{f(4)})^2\mathrm{Li}_2\left(\frac{-p_t^2}{m^2}\right) + e_{f(3)}e_{f(4)}\frac{1}{v}L_{34}(v, y_{34}) \quad \text{(A.9)}$$

with $p_t \equiv p_{t,f(3)} = p_{t,f(3)}$ the common transverse momentum of the leptons, $m_t = \sqrt{p_t^2 + m^2}$ their transverse mass, $y_{34} = y_3 - y_4$ the rapidity difference between the two leptons and

$$L_{34} = \ln\left(\frac{1+v}{1-v}\right)\ln\left(\frac{m_t^2}{m^2}\right) - 2\,\mathrm{Li}_2\left(\frac{2v}{1+v}\right) - \frac{1}{4}\ln^2\left(\frac{1+v}{1-v}\right)$$

$$+ 2\left[\mathrm{Li}_2\left(1 - \sqrt{\frac{1-v}{1+v}}\,e^{y_{34}}\right) + \mathrm{Li}_2\left(1 - \sqrt{\frac{1-v}{1+v}}\,e^{-y_{34}}\right) + \frac{1}{2}\,y_{34}^2\right] \quad \text{(A.10)}$$

in terms of the relative velocity $v = \sqrt{1 - 4\,m^4/s_{34}^2}$.

The mixed QCD-EW radiator functions at lowest order are (see also [102])

$$g_{11}(\lambda, \lambda') = \frac{A^{(1)}\beta_{01}}{4\pi\beta_0'\beta_0^2}\left[\frac{\ln(1-2\lambda')}{1-2\lambda} + \frac{\lambda'}{\lambda-\lambda'}\ln\frac{1-2\lambda'}{1-2\lambda} + \ln(1-2\lambda')\ln\frac{(1-2\lambda)\lambda'}{\lambda'-\lambda}\right.$$

$$\left. + \text{Li}_2\left(\frac{\lambda(1-2\lambda')}{\lambda-\lambda'}\right) - \text{Li}_2\left(\frac{\lambda}{\lambda-\lambda'}\right)\right], \tag{A.11}$$

while $g_{11}'(\lambda, \lambda')$ is obtained from the above function with the replacements $\lambda \leftrightarrow \lambda'$, $\beta_j \leftrightarrow \beta_j'$, $A^{(1)} \to A'^{(1)}$.

Finally, the mixed hard-collinear anomalous dimension can be deduced abelianising the $B^{(2)}$ QCD coefficient [56, 179]:

$$B^{(1,1)} = \sum_{\ell=1}^{2} B_\ell^{(1,1)}, \qquad B_\ell^{(1,1)} = e_{f(\ell)}^2\frac{8}{3}\left(\pi^2 - \frac{3}{4} - 12\,\zeta_3\right). \tag{A.12}$$

References

[1] CDF and D0 collaborations, *2012 Update of the Combination of CDF and D0 Results for the Mass of the W Boson*, `arXiv:1204.0042` [InSPIRE].

[2] ATLAS collaboration, *Measurement of the W-boson mass in pp collisions at $\sqrt{s} = 7$ TeV with the ATLAS detector*, *Eur. Phys. J. C* **78** (2018) 110 [*Erratum ibid.* **78** (2018) 898] [`arXiv:1701.07240`] [InSPIRE].

[3] LHCb collaboration, *Measurement of the W boson mass*, *JHEP* **01** (2022) 036 [`arXiv:2109.01113`] [InSPIRE].

[4] CDF collaboration, *High-precision measurement of the W boson mass with the CDF II detector*, *Science* **376** (2022) 170 [InSPIRE].

[5] ATLAS collaboration, *Improved W boson Mass Measurement using 7 TeV Proton-Proton Collisions with the ATLAS Detector*, ATLAS-CONF-2023-004 (2023) [InSPIRE].

[6] CMS collaboration, *Measurement of the weak mixing angle with the Drell-Yan process in proton-proton collisions at the LHC*, *Phys. Rev. D* **84** (2011) 112002 [`arXiv:1110.2682`] [InSPIRE].

[7] ATLAS collaboration, *Measurement of the forward-backward asymmetry of electron and muon pair-production in pp collisions at $\sqrt{s} = 7$ TeV with the ATLAS detector*, *JHEP* **09** (2015) 049 [`arXiv:1503.03709`] [InSPIRE].

[8] LHCb collaboration, *Measurement of the forward-backward asymmetry in $Z/\gamma^* \to \mu^+\mu^-$ decays and determination of the effective weak mixing angle*, *JHEP* **11** (2015) 190 [`arXiv:1509.07645`] [InSPIRE].

[9] CDF and D0 collaborations, *Tevatron Run II combination of the effective leptonic electroweak mixing angle*, *Phys. Rev. D* **97** (2018) 112007 [`arXiv:1801.06283`] [InSPIRE].

[10] CMS collaboration, *Measurement of the weak mixing angle using the forward-backward asymmetry of Drell-Yan events in pp collisions at 8 TeV*, *Eur. Phys. J. C* **78** (2018) 701 [arXiv:1806.00863] [INSPIRE].

[11] ATLAS collaboration, *Measurement of the effective leptonic weak mixing angle using electron and muon pairs from Z-boson decay in the ATLAS experiment at $\sqrt{s} = 8$ TeV*, ATLAS-CONF-2018-037 (2018) [INSPIRE].

[12] CMS collaboration, *Measurement of the Drell-Yan forward-backward asymmetry and of the effective leptonic weak mixing angle using proton-proton collisions at 13 TeV*, CMS-PAS-SMP-22-010 (2024) [INSPIRE].

[13] ATLAS collaboration, *A precise determination of the strong-coupling constant from the recoil of Z bosons with the ATLAS experiment at $\sqrt{s} = 8$ TeV*, arXiv:2309.12986 [INSPIRE].

[14] ATLAS collaboration, *Measurement of the transverse momentum distribution of Drell-Yan lepton pairs in proton-proton collisions at $\sqrt{s} = 13$ TeV with the ATLAS detector*, *Eur. Phys. J. C* **80** (2020) 616 [arXiv:1912.02844] [INSPIRE].

[15] CMS collaboration, *Measurements of differential Z boson production cross sections in proton-proton collisions at $\sqrt{s} = 13$ TeV*, *JHEP* **12** (2019) 061 [arXiv:1909.04133] [INSPIRE].

[16] LHCb collaboration, *Precision measurement of forward Z boson production in proton-proton collisions at $\sqrt{s} = 13$ TeV*, *JHEP* **07** (2022) 026 [arXiv:2112.07458] [INSPIRE].

[17] CMS collaboration, *Measurement of the mass dependence of the transverse momentum of lepton pairs in Drell-Yan production in proton-proton collisions at $\sqrt{s} = 13$ TeV*, *Eur. Phys. J. C* **83** (2023) 628 [arXiv:2205.04897] [INSPIRE].

[18] ATLAS collaboration, *A precise measurement of the Z-boson double-differential transverse momentum and rapidity distributions in the full phase space of the decay leptons with the ATLAS experiment at $\sqrt{s} = 8$ TeV*, *Eur. Phys. J. C* **84** (2024) 315 [arXiv:2309.09318] [INSPIRE].

[19] LHCb collaboration, *Measurement of the Z boson production cross-section in pp collisions at $\sqrt{s} = 5.02$ TeV*, *JHEP* **02** (2024) 070 [arXiv:2308.12940] [INSPIRE].

[20] ATLAS collaboration, *Precise measurements of W- and Z-boson transverse momentum spectra with the ATLAS detector using pp collisions at $\sqrt{s} = 5.02$ TeV and 13 TeV*, arXiv:2404.06204 [INSPIRE].

[21] G. Altarelli, R.K. Ellis and G. Martinelli, *Large Perturbative Corrections to the Drell-Yan Process in QCD*, *Nucl. Phys. B* **157** (1979) 461 [INSPIRE].

[22] R. Hamberg, W.L. van Neerven and T. Matsuura, *A complete calculation of the order $\alpha - s^2$ correction to the Drell-Yan K factor*, *Nucl. Phys. B* **359** (1991) 343 [INSPIRE].

[23] R.V. Harlander and W.B. Kilgore, *Next-to-next-to-leading order Higgs production at hadron colliders*, *Phys. Rev. Lett.* **88** (2002) 201801 [hep-ph/0201206] [INSPIRE].

[24] C. Anastasiou, L.J. Dixon, K. Melnikov and F. Petriello, *Dilepton rapidity distribution in the Drell-Yan process at NNLO in QCD*, *Phys. Rev. Lett.* **91** (2003) 182002 [hep-ph/0306192] [INSPIRE].

[25] C. Anastasiou, L.J. Dixon, K. Melnikov and F. Petriello, *High precision QCD at hadron colliders: Electroweak gauge boson rapidity distributions at NNLO*, *Phys. Rev. D* **69** (2004) 094008 [hep-ph/0312266] [INSPIRE].

[26] K. Melnikov and F. Petriello, *The W boson production cross section at the LHC through $O(\alpha_s^2)$,* *Phys. Rev. Lett.* **96** (2006) 231803 [`hep-ph/0603182`] [INSPIRE].

[27] K. Melnikov and F. Petriello, *Electroweak gauge boson production at hadron colliders through $O(\alpha_s^2)$,* *Phys. Rev. D* **74** (2006) 114017 [`hep-ph/0609070`] [INSPIRE].

[28] S. Catani et al., *Vector boson production at hadron colliders: a fully exclusive QCD calculation at NNLO,* *Phys. Rev. Lett.* **103** (2009) 082001 [`arXiv:0903.2120`] [INSPIRE].

[29] S. Catani, G. Ferrera and M. Grazzini, *W Boson Production at Hadron Colliders: The Lepton Charge Asymmetry in NNLO QCD,* *JHEP* **05** (2010) 006 [`arXiv:1002.3115`] [INSPIRE].

[30] C. Duhr, F. Dulat and B. Mistlberger, *Drell-Yan Cross Section to Third Order in the Strong Coupling Constant,* *Phys. Rev. Lett.* **125** (2020) 172001 [`arXiv:2001.07717`] [INSPIRE].

[31] C. Duhr, F. Dulat and B. Mistlberger, *Charged current Drell-Yan production at N^3LO,* *JHEP* **11** (2020) 143 [`arXiv:2007.13313`] [INSPIRE].

[32] J. Baglio, C. Duhr, B. Mistlberger and R. Szafron, *Inclusive production cross sections at N^3LO,* *JHEP* **12** (2022) 066 [`arXiv:2209.06138`] [INSPIRE].

[33] X. Chen et al., *Dilepton Rapidity Distribution in Drell-Yan Production to Third Order in QCD,* *Phys. Rev. Lett.* **128** (2022) 052001 [`arXiv:2107.09085`] [INSPIRE].

[34] X. Chen et al., *Third-Order Fiducial Predictions for Drell-Yan Production at the LHC,* *Phys. Rev. Lett.* **128** (2022) 252001 [`arXiv:2203.01565`] [INSPIRE].

[35] X. Chen et al., *Transverse mass distribution and charge asymmetry in W boson production to third order in QCD,* *Phys. Lett. B* **840** (2023) 137876 [`arXiv:2205.11426`] [INSPIRE].

[36] X. Chen et al., *Theory uncertainties in the fiducial Drell-Yan cross section and distributions,* in the proceedings of the *56th Rencontres de Moriond on QCD and High Energy Interactions,* La Thuile, Italy, 19–26 March 2022 [`arXiv:2206.11059`] [INSPIRE].

[37] T. Neumann and J. Campbell, *Fiducial Drell-Yan production at the LHC improved by transverse-momentum resummation at $N^4LL_p + N^3LO$,* *Phys. Rev. D* **107** (2023) L011506 [`arXiv:2207.07056`] [INSPIRE].

[38] J. Campbell and T. Neumann, *Third order QCD predictions for fiducial W-boson production,* *JHEP* **11** (2023) 127 [`arXiv:2308.15382`] [INSPIRE].

[39] S. Camarda, L. Cieri and G. Ferrera, *Drell-Yan lepton-pair production: q_T resummation at N^3LL accuracy and fiducial cross sections at N^3LO,* *Phys. Rev. D* **104** (2021) L111503 [`arXiv:2103.04974`] [INSPIRE].

[40] S. Dittmaier and M. Krämer, *Electroweak radiative corrections to W boson production at hadron colliders,* *Phys. Rev. D* **65** (2002) 073007 [`hep-ph/0109062`] [INSPIRE].

[41] U. Baur and D. Wackeroth, *Electroweak radiative corrections to $p\bar{p} \to W^\pm \to \ell^\pm \nu$ beyond the pole approximation,* *Phys. Rev. D* **70** (2004) 073015 [`hep-ph/0405191`] [INSPIRE].

[42] V.A. Zykunov, *Radiative corrections to the Drell-Yan process at large dilepton invariant masses,* *Phys. Atom. Nucl.* **69** (2006) 1522 [INSPIRE].

[43] A. Arbuzov et al., *One-loop corrections to the Drell-Yan process in SANC. I. The charged current case,* *Eur. Phys. J. C* **46** (2006) 407 [*Erratum ibid.* **50** (2007) 505] [`hep-ph/0506110`] [INSPIRE].

[44] C.M. Carloni Calame, G. Montagna, O. Nicrosini and A. Vicini, *Precision electroweak calculation of the charged current Drell-Yan process,* *JHEP* **12** (2006) 016 [`hep-ph/0609170`] [INSPIRE].

[45] U. Baur et al., *Electroweak radiative corrections to neutral current Drell-Yan processes at hadron colliders*, *Phys. Rev. D* **65** (2002) 033007 [hep-ph/0108274] [INSPIRE].

[46] V.A. Zykunov, *Weak radiative corrections to Drell-Yan process for large invariant mass of di-lepton pair*, *Phys. Rev. D* **75** (2007) 073019 [hep-ph/0509315] [INSPIRE].

[47] C.M. Carloni Calame, G. Montagna, O. Nicrosini and A. Vicini, *Precision electroweak calculation of the production of a high transverse-momentum lepton pair at hadron colliders*, *JHEP* **10** (2007) 109 [arXiv:0710.1722] [INSPIRE].

[48] A. Arbuzov et al., *One-loop corrections to the Drell-Yan process in SANC. (II). The neutral current case*, *Eur. Phys. J. C* **54** (2008) 451 [arXiv:0711.0625] [INSPIRE].

[49] S. Dittmaier and M. Huber, *Radiative corrections to the neutral-current Drell-Yan process in the Standard Model and its minimal supersymmetric extension*, *JHEP* **01** (2010) 060 [arXiv:0911.2329] [INSPIRE].

[50] A. Denner and S. Dittmaier, *Electroweak Radiative Corrections for Collider Physics*, *Phys. Rept.* **864** (2020) 1 [arXiv:1912.06823] [INSPIRE].

[51] S. Dittmaier, A. Huss and C. Schwinn, *Mixed QCD-electroweak $\mathcal{O}(\alpha_s\alpha)$ corrections to Drell-Yan processes in the resonance region: pole approximation and non-factorizable corrections*, *Nucl. Phys. B* **885** (2014) 318 [arXiv:1403.3216] [INSPIRE].

[52] S. Dittmaier, A. Huss and C. Schwinn, *Dominant mixed QCD-electroweak $O(\alpha_s\alpha)$ corrections to Drell-Yan processes in the resonance region*, *Nucl. Phys. B* **904** (2016) 216 [arXiv:1511.08016] [INSPIRE].

[53] S. Dittmaier, A. Huss and J. Schwarz, *Mixed NNLO QCD $\times$ electroweak corrections to single-Z production in pole approximation: differential distributions and forward-backward asymmetry*, *JHEP* **05** (2024) 170 [arXiv:2401.15682] [INSPIRE].

[54] D. de Florian, M. Der and I. Fabre, *QCD$\oplus$QED NNLO corrections to Drell Yan production*, *Phys. Rev. D* **98** (2018) 094008 [arXiv:1805.12214] [INSPIRE].

[55] M. Delto, M. Jaquier, K. Melnikov and R. Röntsch, *Mixed QCD$\otimes$QED corrections to on-shell Z boson production at the LHC*, *JHEP* **01** (2020) 043 [arXiv:1909.08428] [INSPIRE].

[56] L. Cieri, D. de Florian, M. Der and J. Mazzitelli, *Mixed QCD$\otimes$QED corrections to exclusive Drell Yan production using the q_T-subtraction method*, *JHEP* **09** (2020) 155 [arXiv:2005.01315] [INSPIRE].

[57] R. Bonciani, F. Buccioni, R. Mondini and A. Vicini, *Double-real corrections at $\mathcal{O}(\alpha\alpha_s)$ to single gauge boson production*, *Eur. Phys. J. C* **77** (2017) 187 [arXiv:1611.00645] [INSPIRE].

[58] R. Bonciani et al., *NNLO QCD$\times$EW corrections to Z production in the $q\bar{q}$ channel*, *Phys. Rev. D* **101** (2020) 031301 [arXiv:1911.06200] [INSPIRE].

[59] R. Bonciani, F. Buccioni, N. Rana and A. Vicini, *Next-to-Next-to-Leading Order Mixed QCD-Electroweak Corrections to on-Shell Z Production*, *Phys. Rev. Lett.* **125** (2020) 232004 [arXiv:2007.06518] [INSPIRE].

[60] L. Buonocore et al., *Mixed QCD-EW corrections to $pp \to \ell\nu_\ell + X$ at the LHC*, *Phys. Rev. D* **103** (2021) 114012 [arXiv:2102.12539] [INSPIRE].

[61] M. Heller, A. von Manteuffel, R.M. Schabinger and H. Spiesberger, *Mixed EW-QCD two-loop amplitudes for $q\bar{q} \to \ell^+\ell^-$ and γ_5 scheme independence of multi-loop corrections*, *JHEP* **05** (2021) 213 [arXiv:2012.05918] [INSPIRE].

[62] T. Armadillo et al., *Two-loop mixed QCD-EW corrections to neutral current Drell-Yan*, *JHEP* **05** (2022) 072 [arXiv:2201.01754] [InSPIRE].

[63] R. Bonciani et al., *Mixed Strong-Electroweak Corrections to the Drell-Yan Process*, *Phys. Rev. Lett.* **128** (2022) 012002 [arXiv:2106.11953] [InSPIRE].

[64] F. Buccioni et al., *Mixed QCD-electroweak corrections to dilepton production at the LHC in the high invariant mass region*, *JHEP* **06** (2022) 022 [arXiv:2203.11237] [InSPIRE].

[65] A. Banfi et al., *Optimisation of variables for studying dilepton transverse momentum distributions at hadron colliders*, *Eur. Phys. J. C* **71** (2011) 1600 [arXiv:1009.1580] [InSPIRE].

[66] G. Parisi and R. Petronzio, *Small Transverse Momentum Distributions in Hard Processes*, *Nucl. Phys. B* **154** (1979) 427 [InSPIRE].

[67] J.C. Collins, D.E. Soper and G.F. Sterman, *Transverse Momentum Distribution in Drell-Yan Pair and W and Z Boson Production*, *Nucl. Phys. B* **250** (1985) 199 [InSPIRE].

[68] C. Balazs, J.-W. Qiu and C.P. Yuan, *Effects of QCD resummation on distributions of leptons from the decay of electroweak vector bosons*, *Phys. Lett. B* **355** (1995) 548 [hep-ph/9505203] [InSPIRE].

[69] C. Balazs and C.P. Yuan, *Soft gluon effects on lepton pairs at hadron colliders*, *Phys. Rev. D* **56** (1997) 5558 [hep-ph/9704258] [InSPIRE].

[70] S. Catani, D. de Florian and M. Grazzini, *Universality of nonleading logarithmic contributions in transverse momentum distributions*, *Nucl. Phys. B* **596** (2001) 299 [hep-ph/0008184] [InSPIRE].

[71] G. Bozzi et al., *Transverse-momentum resummation: A perturbative study of Z production at the Tevatron*, *Nucl. Phys. B* **815** (2009) 174 [arXiv:0812.2862] [InSPIRE].

[72] G. Bozzi et al., *Production of Drell-Yan lepton pairs in hadron collisions: Transverse-momentum resummation at next-to-next-to-leading logarithmic accuracy*, *Phys. Lett. B* **696** (2011) 207 [arXiv:1007.2351] [InSPIRE].

[73] T. Becher and M. Neubert, *Drell-Yan Production at Small q_T, Transverse Parton Distributions and the Collinear Anomaly*, *Eur. Phys. J. C* **71** (2011) 1665 [arXiv:1007.4005] [InSPIRE].

[74] A. Banfi, M. Dasgupta, S. Marzani and L. Tomlinson, *Probing the low transverse momentum domain of Z production with novel variables*, *JHEP* **01** (2012) 044 [arXiv:1110.4009] [InSPIRE].

[75] M.G. Echevarria, A. Idilbi and I. Scimemi, *Factorization Theorem For Drell-Yan At Low q_T And Transverse Momentum Distributions On-The-Light-Cone*, *JHEP* **07** (2012) 002 [arXiv:1111.4996] [InSPIRE].

[76] A. Banfi, M. Dasgupta, S. Marzani and L. Tomlinson, *Predictions for Drell-Yan ϕ^* and Q_T observables at the LHC*, *Phys. Lett. B* **715** (2012) 152 [arXiv:1205.4760] [InSPIRE].

[77] S. Catani, D. de Florian, G. Ferrera and M. Grazzini, *Vector boson production at hadron colliders: transverse-momentum resummation and leptonic decay*, *JHEP* **12** (2015) 047 [arXiv:1507.06937] [InSPIRE].

[78] P.F. Monni, E. Re and P. Torrielli, *Higgs Transverse-Momentum Resummation in Direct Space*, *Phys. Rev. Lett.* **116** (2016) 242001 [arXiv:1604.02191] [InSPIRE].

[79] J.P. Isaacson, *ResBos2: precision resummation for the LHC ERA*, Ph.D. Thesis, Michigan State University (2017) [DOI:10.25335/M5DG44] [InSPIRE].

[80] F. Coradeschi and T. Cridge, *reSolve — A transverse momentum resummation tool*, *Comput. Phys. Commun.* **238** (2019) 262 [arXiv:1711.02083] [INSPIRE].

[81] D. Kang, C. Lee and V. Vaidya, *A fast and accurate method for perturbative resummation of transverse momentum-dependent observables*, *JHEP* **04** (2018) 149 [arXiv:1710.00078] [INSPIRE].

[82] I. Scimemi and A. Vladimirov, *Analysis of vector boson production within TMD factorization*, *Eur. Phys. J. C* **78** (2018) 89 [arXiv:1706.01473] [INSPIRE].

[83] S. Camarda et al., *DYTurbo: Fast predictions for Drell-Yan processes*, *Eur. Phys. J. C* **80** (2020) 251 [*Erratum ibid.* **80** (2020) 440] [arXiv:1910.07049] [INSPIRE].

[84] W. Bizoń et al., *Momentum-space resummation for transverse observables and the Higgs $p_\perp$ at $N^3LL+NNLO$*, *JHEP* **02** (2018) 108 [arXiv:1705.09127] [INSPIRE].

[85] W. Bizoń et al., *Fiducial distributions in Higgs and Drell-Yan production at $N^3LL+NNLO$*, *JHEP* **12** (2018) 132 [arXiv:1805.05916] [INSPIRE].

[86] W. Bizoń et al., *The transverse momentum spectrum of weak gauge bosons at $N^3LL+NNLO$*, *Eur. Phys. J. C* **79** (2019) 868 [arXiv:1905.05171] [INSPIRE].

[87] A. Bacchetta et al., *Transverse-momentum-dependent parton distributions up to N^3LL from Drell-Yan data*, *JHEP* **07** (2020) 117 [arXiv:1912.07550] [INSPIRE].

[88] T. Becher and M. Hager, *Event-Based Transverse Momentum Resummation*, *Eur. Phys. J. C* **79** (2019) 665 [arXiv:1904.08325] [INSPIRE].

[89] M.A. Ebert, J.K.L. Michel, I.W. Stewart and F.J. Tackmann, *Drell-Yan q_T resummation of fiducial power corrections at N^3LL*, *JHEP* **04** (2021) 102 [arXiv:2006.11382] [INSPIRE].

[90] T. Becher and T. Neumann, *Fiducial q_T resummation of color-singlet processes at $N^3LL+NNLO$*, *JHEP* **03** (2021) 199 [arXiv:2009.11437] [INSPIRE].

[91] E. Re, L. Rottoli and P. Torrielli, *Fiducial Higgs and Drell-Yan distributions at $N^3LL'+NNLO$ with RadISH*, arXiv:2104.07509 [DOI:10.1007/JHEP09(2021)108] [INSPIRE].

[92] W.-L. Ju and M. Schönherr, *The q_T and $\Delta\phi$ spectra in W and Z production at the LHC at $N^3LL'+N^2LO$*, *JHEP* **10** (2021) 088 [arXiv:2106.11260] [INSPIRE].

[93] J. Isaacson, Y. Fu and C.-P. Yuan, *Improving ResBos for the precision needs of the LHC*, arXiv:2311.09916 [INSPIRE].

[94] S. Camarda, L. Cieri and G. Ferrera, *Drell-Yan lepton-pair production: q_T resummation at N^4LL accuracy*, *Phys. Lett. B* **845** (2023) 138125 [arXiv:2303.12781] [INSPIRE].

[95] V. Moos, I. Scimemi, A. Vladimirov and P. Zurita, *Extraction of unpolarized transverse momentum distributions from the fit of Drell-Yan data at N^4LL*, *JHEP* **05** (2024) 036 [arXiv:2305.07473] [INSPIRE].

[96] Q.-H. Cao and C.P. Yuan, *Combined effect of QCD resummation and QED radiative correction to W boson observables at the Tevatron*, *Phys. Rev. Lett.* **93** (2004) 042001 [hep-ph/0401026] [INSPIRE].

[97] G. Balossini et al., *Combination of electroweak and QCD corrections to single W production at the Fermilab Tevatron and the CERN LHC*, *JHEP* **01** (2010) 013 [arXiv:0907.0276] [INSPIRE].

[98] C.M. Carloni Calame et al., *Precision Measurement of the W-Boson Mass: Theoretical Contributions and Uncertainties*, *Phys. Rev. D* **96** (2017) 093005 [arXiv:1612.02841] [INSPIRE].

[99] D. de Florian, G.F.R. Sborlini and G. Rodrigo, *QED corrections to the Altarelli-Parisi splitting functions*, *Eur. Phys. J. C* **76** (2016) 282 [arXiv:1512.00612] [InSPIRE].

[100] D. de Florian, G.F.R. Sborlini and G. Rodrigo, *Two-loop QED corrections to the Altarelli-Parisi splitting functions*, *JHEP* **10** (2016) 056 [arXiv:1606.02887] [InSPIRE].

[101] G. Billis, F.J. Tackmann and J. Talbert, *Higher-Order Sudakov Resummation in Coupled Gauge Theories*, *JHEP* **03** (2020) 182 [arXiv:1907.02971] [InSPIRE].

[102] L. Cieri, G. Ferrera and G.F.R. Sborlini, *Combining QED and QCD transverse-momentum resummation for Z boson production at hadron colliders*, *JHEP* **08** (2018) 165 [arXiv:1805.11948] [InSPIRE].

[103] A. Autieri, L. Cieri, G. Ferrera and G.F.R. Sborlini, *Combining QED and QCD transverse-momentum resummation for W and Z boson production at hadron colliders*, *JHEP* **07** (2023) 104 [arXiv:2302.05403] [InSPIRE].

[104] P. Golonka and Z. Was, *PHOTOS Monte Carlo: A precision tool for QED corrections in Z and W decays*, *Eur. Phys. J. C* **45** (2006) 97 [hep-ph/0506026] [InSPIRE].

[105] C.M. Carloni Calame, G. Montagna, O. Nicrosini and M. Treccani, *Higher order QED corrections to W boson mass determination at hadron colliders*, *Phys. Rev. D* **69** (2004) 037301 [hep-ph/0303102] [InSPIRE].

[106] C.M. Carloni Calame, G. Montagna, O. Nicrosini and M. Treccani, *Multiple photon corrections to the neutral-current Drell-Yan process*, *JHEP* **05** (2005) 019 [hep-ph/0502218] [InSPIRE].

[107] T. Sjöstrand et al., *An introduction to PYTHIA 8.2*, *Comput. Phys. Commun.* **191** (2015) 159 [arXiv:1410.3012] [InSPIRE].

[108] N. Fischer, S. Prestel, M. Ritzmann and P. Skands, *Vincia for Hadron Colliders*, *Eur. Phys. J. C* **76** (2016) 589 [arXiv:1605.06142] [InSPIRE].

[109] R. Kleiss and R. Verheyen, *Final-state QED Multipole Radiation in Antenna Parton Showers*, *JHEP* **11** (2017) 182 [arXiv:1709.04485] [InSPIRE].

[110] J. Bellm et al., *Herwig 7.0/Herwig++ 3.0 release note*, *Eur. Phys. J. C* **76** (2016) 196 [arXiv:1512.01178] [InSPIRE].

[111] G. Bewick et al., *Herwig 7.3 Release Note*, arXiv:2312.05175 [InSPIRE].

[112] M. Schönherr and F. Krauss, *Soft Photon Radiation in Particle Decays in SHERPA*, *JHEP* **12** (2008) 018 [arXiv:0810.5071] [InSPIRE].

[113] F. Krauss, J.M. Lindert, R. Linten and M. Schönherr, *Accurate simulation of W, Z and Higgs boson decays in Sherpa*, *Eur. Phys. J. C* **79** (2019) 143 [arXiv:1809.10650] [InSPIRE].

[114] SHERPA collaboration, *Event Generation with Sherpa 2.2*, *SciPost Phys.* **7** (2019) 034 [arXiv:1905.09127] [InSPIRE].

[115] C. Bernaciak and D. Wackeroth, *Combining NLO QCD and Electroweak Radiative Corrections to W boson Production at Hadron Colliders in the POWHEG Framework*, *Phys. Rev. D* **85** (2012) 093003 [arXiv:1201.4804] [InSPIRE].

[116] L. Barze et al., *Implementation of electroweak corrections in the POWHEG BOX: single W production*, *JHEP* **04** (2012) 037 [arXiv:1202.0465] [InSPIRE].

[117] L. Barze et al., *Neutral current Drell-Yan with combined QCD and electroweak corrections in the POWHEG BOX*, *Eur. Phys. J. C* **73** (2013) 2474 [arXiv:1302.4606] [InSPIRE].

[118] M. Chiesa, C.L. Del Pio and F. Piccinini, *On electroweak corrections to neutral current Drell-Yan with the POWHEG BOX*, *Eur. Phys. J. C* **84** (2024) 539 [arXiv:2402.14659] [INSPIRE].

[119] A. Mück and L. Oymanns, *Resonace-improved parton-shower matching for the Drell-Yan process including electroweak corrections*, *JHEP* **05** (2017) 090 [arXiv:1612.04292] [INSPIRE].

[120] L. Rottoli, P. Torrielli and A. Vicini, *Determination of the W-boson mass at hadron colliders*, *Eur. Phys. J. C* **83** (2023) 948 [arXiv:2301.04059] [INSPIRE].

[121] P. Torrielli, L. Rottoli and A. Vicini, *A new observable for W-mass determination*, *PoS* **RADCOR2023** (2024) 038 [arXiv:2308.15993] [INSPIRE].

[122] P.F. Monni, L. Rottoli and P. Torrielli, *Higgs transverse momentum with a jet veto: a double-differential resummation*, *Phys. Rev. Lett.* **124** (2020) 252001 [arXiv:1909.04704] [INSPIRE].

[123] S. Kallweit, E. Re, L. Rottoli and M. Wiesemann, *Accurate single- and double-differential resummation of colour-singlet processes with MATRIX+RADISH: W⁺W⁻ production at the LHC*, *JHEP* **12** (2020) 147 [arXiv:2004.07720] [INSPIRE].

[124] A. Banfi, G.P. Salam and G. Zanderighi, *Semi-numerical resummation of event shapes*, *JHEP* **01** (2002) 018 [hep-ph/0112156] [INSPIRE].

[125] A. Banfi, G.P. Salam and G. Zanderighi, *Generalized resummation of QCD final state observables*, *Phys. Lett. B* **584** (2004) 298 [hep-ph/0304148] [INSPIRE].

[126] A. Banfi, G.P. Salam and G. Zanderighi, *Principles of general final-state resummation and automated implementation*, *JHEP* **03** (2005) 073 [hep-ph/0407286] [INSPIRE].

[127] G. Altarelli and G. Parisi, *Asymptotic Freedom in Parton Language*, *Nucl. Phys. B* **126** (1977) 298 [INSPIRE].

[128] V.N. Gribov and L.N. Lipatov, *Deep inelastic e p scattering in perturbation theory*, *Sov. J. Nucl. Phys.* **15** (1972) 438 [INSPIRE].

[129] Y.L. Dokshitzer, *Calculation of the Structure Functions for Deep Inelastic Scattering and e⁺e⁻ Annihilation by Perturbation Theory in Quantum Chromodynamics*, *Sov. Phys. JETP* **46** (1977) 641 [INSPIRE].

[130] S. Catani and M. Grazzini, *Higgs Boson Production at Hadron Colliders: Hard-Collinear Coefficients at the NNLO*, *Eur. Phys. J. C* **72** (2012) 2013 [*Erratum ibid.* **72** (2012) 2132] [arXiv:1106.4652] [INSPIRE].

[131] S. Catani et al., *Vector boson production at hadron colliders: hard-collinear coefficients at the NNLO*, *Eur. Phys. J. C* **72** (2012) 2195 [arXiv:1209.0158] [INSPIRE].

[132] T. Gehrmann, T. Luebbert and L.L. Yang, *Calculation of the transverse parton distribution functions at next-to-next-to-leading order*, *JHEP* **06** (2014) 155 [arXiv:1403.6451] [INSPIRE].

[133] T. Lübbert, J. Oredsson and M. Stahlhofen, *Rapidity renormalized TMD soft and beam functions at two loops*, *JHEP* **03** (2016) 168 [arXiv:1602.01829] [INSPIRE].

[134] M.G. Echevarria, I. Scimemi and A. Vladimirov, *Unpolarized Transverse Momentum Dependent Parton Distribution and Fragmentation Functions at next-to-next-to-leading order*, *JHEP* **09** (2016) 004 [arXiv:1604.07869] [INSPIRE].

[135] Y. Li and H.X. Zhu, *Bootstrapping Rapidity Anomalous Dimensions for Transverse-Momentum Resummation*, *Phys. Rev. Lett.* **118** (2017) 022004 [arXiv:1604.01404] [INSPIRE].

[136] A.A. Vladimirov, *Correspondence between Soft and Rapidity Anomalous Dimensions*, *Phys. Rev. Lett.* **118** (2017) 062001 [`arXiv:1610.05791`] [InSPIRE].

[137] S. Moch et al., *Four-Loop Non-Singlet Splitting Functions in the Planar Limit and Beyond*, *JHEP* **10** (2017) 041 [`arXiv:1707.08315`] [InSPIRE].

[138] S. Moch et al., *On quartic colour factors in splitting functions and the gluon cusp anomalous dimension*, *Phys. Lett. B* **782** (2018) 627 [`arXiv:1805.09638`] [InSPIRE].

[139] R.N. Lee, A.V. Smirnov, V.A. Smirnov and M. Steinhauser, *Four-loop quark form factor with quartic fundamental colour factor*, *JHEP* **02** (2019) 172 [`arXiv:1901.02898`] [InSPIRE].

[140] M.-X. Luo, T.-Z. Yang, H.X. Zhu and Y.J. Zhu, *Transverse Parton Distribution and Fragmentation Functions at NNLO: the Gluon Case*, *JHEP* **01** (2020) 040 [`arXiv:1909.13820`] [InSPIRE].

[141] J.M. Henn, G.P. Korchemsky and B. Mistlberger, *The full four-loop cusp anomalous dimension in $\mathcal{N} = 4$ super Yang-Mills and QCD*, *JHEP* **04** (2020) 018 [`arXiv:1911.10174`] [InSPIRE].

[142] R. Brüser, A. Grozin, J.M. Henn and M. Stahlhofen, *Matter dependence of the four-loop QCD cusp anomalous dimension: from small angles to all angles*, *JHEP* **05** (2019) 186 [`arXiv:1902.05076`] [InSPIRE].

[143] J.M. Henn, T. Peraro, M. Stahlhofen and P. Wasser, *Matter dependence of the four-loop cusp anomalous dimension*, *Phys. Rev. Lett.* **122** (2019) 201602 [`arXiv:1901.03693`] [InSPIRE].

[144] M.-X. Luo, T.-Z. Yang, H.X. Zhu and Y.J. Zhu, *Quark Transverse Parton Distribution at the Next-to-Next-to-Next-to-Leading Order*, *Phys. Rev. Lett.* **124** (2020) 092001 [`arXiv:1912.05778`] [InSPIRE].

[145] A. von Manteuffel, E. Panzer and R.M. Schabinger, *Cusp and collinear anomalous dimensions in four-loop QCD from form factors*, *Phys. Rev. Lett.* **124** (2020) 162001 [`arXiv:2002.04617`] [InSPIRE].

[146] M.A. Ebert, B. Mistlberger and G. Vita, *Transverse momentum dependent PDFs at N^3LO*, *JHEP* **09** (2020) 146 [`arXiv:2006.05329`] [InSPIRE].

[147] M.-X. Luo, T.-Z. Yang, H.X. Zhu and Y.J. Zhu, *Unpolarized quark and gluon TMD PDFs and FFs at N^3LO*, *JHEP* **06** (2021) 115 [`arXiv:2012.03256`] [InSPIRE].

[148] S. Catani, M. Grazzini and A. Torre, *Transverse-momentum resummation for heavy-quark hadroproduction*, *Nucl. Phys. B* **890** (2014) 518 [`arXiv:1408.4564`] [InSPIRE].

[149] P. Sun, C.-P. Yuan and F. Yuan, *Transverse Momentum Resummation for Dijet Correlation in Hadronic Collisions*, *Phys. Rev. D* **92** (2015) 094007 [`arXiv:1506.06170`] [InSPIRE].

[150] P. Sun, J. Isaacson, C.-P. Yuan and F. Yuan, *Resummation of High Order Corrections in Higgs Boson Plus Jet Production at the LHC*, *Phys. Lett. B* **769** (2017) 57 [`arXiv:1602.08133`] [InSPIRE].

[151] P. Sun, B. Yan, C.-P. Yuan and F. Yuan, *Resummation of High Order Corrections in Z Boson Plus Jet Production at the LHC*, *Phys. Rev. D* **100** (2019) 054032 [`arXiv:1810.03804`] [InSPIRE].

[152] Y.-T. Chien, D.Y. Shao and B. Wu, *Resummation of Boson-Jet Correlation at Hadron Colliders*, *JHEP* **11** (2019) 025 [`arXiv:1905.01335`] [InSPIRE].

[153] L. Buonocore, M. Grazzini, J. Haag and L. Rottoli, *Transverse-momentum resummation for boson plus jet production at hadron colliders*, *Eur. Phys. J. C* **82** (2022) 27 [`arXiv:2110.06913`] [InSPIRE].

[154] S. Actis et al., *RECOLA: REcursive Computation of One-Loop Amplitudes*, *Comput. Phys. Commun.* **214** (2017) 140 [arXiv:1605.01090] [INSPIRE].

[155] A. Denner, J.-N. Lang and S. Uccirati, *Recola2: REcursive Computation of One-Loop Amplitudes 2*, *Comput. Phys. Commun.* **224** (2018) 346 [arXiv:1711.07388] [INSPIRE].

[156] A. Manohar, P. Nason, G.P. Salam and G. Zanderighi, *How bright is the proton? A precise determination of the photon parton distribution function*, *Phys. Rev. Lett.* **117** (2016) 242002 [arXiv:1607.04266] [INSPIRE].

[157] A. Denner, S. Dittmaier, M. Roth and L.H. Wieders, *Electroweak corrections to charged-current $e^+e^- \to 4$ fermion processes: Technical details and further results*, *Nucl. Phys. B* **724** (2005) 247 [hep-ph/0505042] [INSPIRE].

[158] NNPDF collaboration, *Illuminating the photon content of the proton within a global PDF analysis*, *SciPost Phys.* **5** (2018) 008 [arXiv:1712.07053] [INSPIRE].

[159] A. Buckley et al., *LHAPDF6: parton density access in the LHC precision era*, *Eur. Phys. J. C* **75** (2015) 132 [arXiv:1412.7420] [INSPIRE].

[160] G.P. Salam and J. Rojo, *A Higher Order Perturbative Parton Evolution Toolkit (HOPPET)*, *Comput. Phys. Commun.* **180** (2009) 120 [arXiv:0804.3755] [INSPIRE].

[161] M. Grazzini, S. Kallweit and M. Wiesemann, *Fully differential NNLO computations with MATRIX*, *Eur. Phys. J. C* **78** (2018) 537 [arXiv:1711.06631] [INSPIRE].

[162] S. Catani and M. Grazzini, *An NNLO subtraction formalism in hadron collisions and its application to Higgs boson production at the LHC*, *Phys. Rev. Lett.* **98** (2007) 222002 [hep-ph/0703012] [INSPIRE].

[163] L. Buonocore, S. Kallweit, L. Rottoli and M. Wiesemann, *Linear power corrections for two-body kinematics in the qT subtraction formalism*, *Phys. Lett. B* **829** (2022) 137118 [arXiv:2111.13661] [INSPIRE].

[164] S. Camarda, L. Cieri and G. Ferrera, *Fiducial perturbative power corrections within the q_T subtraction formalism*, *Eur. Phys. J. C* **82** (2022) 575 [arXiv:2111.14509] [INSPIRE].

[165] L. Buonocore, M. Grazzini and F. Tramontano, *The q_T subtraction method: electroweak corrections and power suppressed contributions*, *Eur. Phys. J. C* **80** (2020) 254 [arXiv:1911.10166] [INSPIRE].

[166] G. Bozzi, S. Catani, D. de Florian and M. Grazzini, *Transverse-momentum resummation and the spectrum of the Higgs boson at the LHC*, *Nucl. Phys. B* **737** (2006) 73 [hep-ph/0508068] [INSPIRE].

[167] A. Banfi, G.P. Salam and G. Zanderighi, *NLL+NNLO predictions for jet-veto efficiencies in Higgs-boson and Drell-Yan production*, *JHEP* **06** (2012) 159 [arXiv:1203.5773] [INSPIRE].

[168] NNPDF collaboration, *Parton distributions from high-precision collider data*, *Eur. Phys. J. C* **77** (2017) 663 [arXiv:1706.00428] [INSPIRE].

[169] S. Catani and B.R. Webber, *Infrared safe but infinite: Soft gluon divergences inside the physical region*, *JHEP* **10** (1997) 005 [hep-ph/9710333] [INSPIRE].

[170] S. Alioli et al., *Precision studies of observables in $pp \to W \to l\nu_l$ and $pp \to \gamma, Z \to l^+l^-$ processes at the LHC*, *Eur. Phys. J. C* **77** (2017) 280 [arXiv:1606.02330] [INSPIRE].

[171] ATLAS collaboration, *Measurement of the Z/γ^* boson transverse momentum distribution in pp collisions at $\sqrt{s} = 7$ TeV with the ATLAS detector*, *JHEP* **09** (2014) 145 [arXiv:1406.3660] [INSPIRE].

[172] P. Nason, *A new method for combining NLO QCD with shower Monte Carlo algorithms*, *JHEP* **11** (2004) 040 [`hep-ph/0409146`] [ɪɴSPIRE].

[173] S. Alioli, P. Nason, C. Oleari and E. Re, *A general framework for implementing NLO calculations in shower Monte Carlo programs: the POWHEG BOX*, *JHEP* **06** (2010) 043 [`arXiv:1002.2581`] [ɪɴSPIRE].

[174] T. Binoth et al., *A Proposal for a Standard Interface between Monte Carlo Tools and One-Loop Programs*, *Comput. Phys. Commun.* **181** (2010) 1612 [`arXiv:1001.1307`] [ɪɴSPIRE].

[175] S. Alioli et al., *Update of the Binoth Les Houches Accord for a standard interface between Monte Carlo tools and one-loop programs*, *Comput. Phys. Commun.* **185** (2014) 560 [`arXiv:1308.3462`] [ɪɴSPIRE].

[176] A. Gehrmann-De Ridder et al., *Next-to-Next-to-Leading-Order QCD Corrections to the Transverse Momentum Distribution of Weak Gauge Bosons*, *Phys. Rev. Lett.* **120** (2018) 122001 [`arXiv:1712.07543`] [ɪɴSPIRE].

[177] S. Alioli, P. Nason, C. Oleari and E. Re, *NLO vector-boson production matched with shower in POWHEG*, *JHEP* **07** (2008) 060 [`arXiv:0805.4802`] [ɪɴSPIRE].

[178] Particle Data Group collaboration, *Review of Particle Physics*, *PTEP* **2022** (2022) 083C01 [ɪɴSPIRE].

[179] L. Buonocore, *Ultimate Precision for the Drell-Yan Process: Mixed QCDxQED(EW) Corrections, Final State Radiation and Power Suppressed Contributions*, Ph.D. Thesis, Università degli Studi di Napoli Federico II, Universität of Zürich (2020) [ɪɴSPIRE].